JOURNAL OF COASTAL AND HYDRAULIC STRUCTURES

Vol. 6, 2026, 51

Re-analysis of the deformation of rock-based scour protections around monopiles exposed to waves and current

Anders Wedel Nielsen [1*]

Abstract

Publicly available data on deformation of scour protections around monopiles has been collected, reviewed, and re-analysed. The review showed that the studies published over the past two decades are comparable and provide results that are overall coherent. The reanalysed data, all based on physical model tests, has been analysed both in qualitative and quantitative ways. The qualitative analysis shows that the deformation patterns of the tests can be uniquely classified based on Shields number and wave-current ratio, while the effect of the, rather low, KC-numbers covered by the data was negligible. The quantitative analysis showed that the magnitude of the deformation follows the same trend as the qualitative analysis. Finally, an analysis of the time scale of the deformation shows an overall trend with regards to wave-current ratio similar to what is reported for live-bed scour, although the time scales are longer. Based on the analysis formulas to predict the time scale and equilibrium deformation of the scour protection are proposed. Based on these formulas it is demonstrated that a time step model can be used to predict the development of the deformation over time. A discussion of potential issues with this method, primarily due to limited available data, and how to reduce the risks associated with these issues are provided as well.

Keywords

Scour protection stability, scour protection of monopiles, clear water scour, time scale of scour protection deformation

[1]NIRAS, Allerød, Denmark (former address: DHI A/S, Hørsholm, Denmark)
[*]awni@niras.dk

Research Article. **Submitted:** 23 March 2025. **Reviewed:** 5 October 2025. **Accepted** after double-blind review: 26 November 2025. **Published:** 21 January 2026.

DOI: 10.59490/jchs.2025.0051

Cite as: Nielsen, A.W., Re-analysis of the deformation of rock-based scour protections around monopiles exposed to waves and current, Journal of Coastal and Hydraulic Structures, 51, DOI: 10.59490/jchs.2025.0051

The Journal of Coastal and Hydraulic Structures is a community-based, free, and open access journal for the dissemination of high-quality knowledge on the engineering science of coastal and hydraulic structures. This paper has been written and reviewed with care. However, the authors and the journal do not accept any liability which might arise from use of its contents. Copyright © 2026 by the authors. This journal paper is published under a CC BY 4.0 license, which allows anyone to redistribute, mix and adapt, as long as credit is given to the authors.

ISSN: 2667-047X online

1 Introduction

Over the past two to three decades there have been significant advancement in the understanding of scour protections around monopiles exposed to waves and current. This has, to a large degree, been driven by the rapid growth of the offshore wind industry over the same period of time and the need for constant optimisations of all parts of the wind farms, including the scour protections, to sustain this growth. This need for optimisation of the scour protections has resulted in multiple studies of the mechanisms related to the scour protection. Studies of the edge scour was reported by Raaijmakers et al. (2007), de Sonneville et al. (2012) and Petersen et al. (2015) and for prototype applications by Raaijmakers et al. (2010), Whitehouse et al. (2011), and Petersen et al. (2015). The sinking of the scour protection adjacent to the monopile was extensively studied by Nielsen et al. (2010, 2011, 2013, 2014, 2015) and Nielsen and Petersen (2018), as a reaction to the sinking reported at Horns Rev 1 OWF (Hansen et al., 2007). De Sonneville et al. (2014); Schendel and Schlurmann (2019) also contributed to the knowledge regarding sinking. Many of these studies, in particular de Sonneville et al. (2012), Petersen et al. (2015), and Nielsen and Petersen (2018), formed the core part

of the Recommended Practice on scour protection of monopiles - DNV-RP-0618 (DNV, 2022) within edge scour and sinking of the scour protection.

Even before the previously mentioned studies the stability of the armour rock was studied extensively. Den Boon et al. (2004) was among the first to study stability of scour protections around monopiles, followed by the studies by de Vos (2008) and de Vos et al. (2011, 2012), as well as Schendel et al. (2014), de Schoesitter et al. (2014), Whitehouse et al. (2014), and Riezebos et al. (2016). However, despite the large amount of data provided by these studies it was not possible to draw a solid conclusion regarding the requirements of an optimised functional design of armour rock for scour protections of monopiles. In the most recent years a large number of studies have been presented providing additional data and knowledge: Ferradosa (2018), Arboleda Chavez et al. (2019), Nielsen and Petersen (2019), Mayall et al. (2020), Wu et al. (2020), Chambel et al. (2023), Nielsen et al. (2023), Broekema et al. (2024), and not least Deltares (2024), but, again without a solid conclusion.

In addition to the actual studies of armour rock stability around monopiles, studies of clear water scour around monopiles have been reviewed as both are governed by similar processes. Studies of clear water scour have been reported by Baker (1986) (via Melville and Sutherland (1988)), Schendel et al. (2018), and de Lemos et al. (2023) in the case of steady current. In the case of waves, clear water scour was studied extensively by Umeda (2011, 2013) for regular and irregular waves, respectively, as well as by Corvaro et al. (2018) for both regular and irregular waves. In addition to the tests of scour protections around monopiles, results of physical model tests of scour protections of tripods were reported in the same period, e.g. Sarmiento et al. (2021).

This review and re-analysis show that the data from the different studies can be presented as function of the Shields and u_{cw}-numbers in line with the study by Nielsen and Petersen (2019). This is the case both when the results are presented in qualitative terms (deformation pattern) and quantitative (deformation depth relative to pile diameter). Opposite findings of Broekema et al. (2024), the deformation is found to be practically independent of the KC-number in the covered range ($0.5 < KC < 5.5$), as also found in Nielsen and Petersen (2019). This corresponds well with live-bed conditions where the variation of the relative scour depth with KC also appears to be small, in the order of magnitude $10^{-3} < S_{eq}/D_p < 10^{-2}$ for $2 < KC < 6$, see Sumer and Fredsøe (2001a). However, given the typical ratio between rock size and pile diameter, D_{50}/D_p in the order of magnitude 10^{-2}, this variation in deformation depth can hardly be seen for a scour protection. The available range of KC-numbers ($0.5 < KC < 5.5$) is also the relevant range for many coastal and offshore applications including monopile and jacket foundations for wind, oil and gas.

The time scale of the deformation and clear water scour has been determined for available tests with sufficient data. The results show that the non-dimensional time scale follows the same trend as for live-bed scour with relatively short non-dimensional time scales for wave alone and steady current and longer time scale for combined waves and current. However, the non-dimensional time scale of the scour protection deformation and clear water scour appears to be indicatively 5 to 1000 times longer than for live-bed conditions, primarily depending on the current-wave ratio. It is noted that the time scales for u_{cw} around 0.4 covers a significant range. It has not been possible to identify the reason, but it may be the general uncertainty of the estimated time scales. Based on the results of a time step model it was found that the increase of the time scale relative to live-bed conditions appeared in the lower end of the range given above.

Based on the findings, formulas for prediction of equilibrium deformation and time scale of the deformation of the scour protection around monopiles are proposed. It is, furthermore, demonstrated that these formulas can be used in a time step model to predict the development of the deformation of the scour protection over time in a similar way as done by e.g. Nielsen and Hansen (2007); Raaijmakers and Rudolph (2008); Harris et al. (2010); Silva-Muñoz and Broekema (2025) for scour. It should, however, be noted that the data for the parametrisations of the equilibrium deformation and time scale is not well distributed so interpolations of spans with no data has been necessary. This may of course impact the accuracy of the model in some cases; this and the impact of the general uncertainty of the parametrisations must be kept in mind if applying the model for design purposes, and it is strongly recommended to evaluate the results carefully.

The present study is largely based on data from Deltares (2024) and the dataset is therefore frequently referenced. However, the dataset is very large, involving many subjects so only a part of the entire dataset is relevant for this study. The relevant part is almost exclusively described in Deltares (2023a), but a minor part is covered by Deltares (2023b). To avoid long explanations every time a reference to the dataset is given, the reference "Deltares (2024)" is implicit to the part covered by Deltares (2023a) and it is specifically mentioned when data from the part covered by Deltares (2023b) is applied.

Finally, a reader's guide is given here. This article is longer than most articles and therefore it may be harder to get and keep the overview of content. Section 2 presents the recent studies that forms the basis of the work and how different studies are applied; primarily divided into 1) quantitative studies of stability of armour rock, 2) quantitative studies of the size of deformation of the scour protection, and 3) qualitative studies of the mechanism of scour armour

layer deformation.

The re-analysis of the data is presented in Sec. 3. This is divided into five parts: Sec. 3.1 presents a qualitative interpretation focusing on the pattern of the deformation of the scour protection and a quantitative interpretation is given in Sec. 3.2, including a description of the selection of the data suitable for this analysis, followed by the proposed parametrisation of the quantitative deformation in Sec. 3.3. The time scale of the deformation is investigated in Sec. 3.4, where a parametrisation of the time scale is also proposed. Finally, a time step model is presented in Sec. 3.5 where it is also compared to results of physical model tests.

Comparison with different other design criteria is given in Sec. 4. This covers the criteria proposed by den Boon et al. (2004), de Vos et al. (2012), Broekema et al. (2024), and Nielsen and Petersen (2019). Sec. 5 covers some remarks regarding the practical application of the results and Sec. 6 gives the overall conclusions. Three appendicies (A to C) outline the applied calculation methods and procedures.

2 Recent studies of stability of armour rock around monopiles

As mentioned in the introduction several studies of armour rock stability have been published over the past decades. Although all the studies had aimed at improving the understanding of the stability of armour rock, the focus have varied between the different key studies. In this section the methodologies and contributions of the different studies will be reviewed and discussed. This review and discussion will form the basis of a reanalysis of the available data considering all the relevant studies.

Studies relevant for armour rock stability can roughly be divided into three categories which are described in more details in Sec. 2.1 to 2.3:

1. Quantitative studies of stability of armour rock
2. Quantitative studies of the size of deformation of the scour protection
3. Qualitative studies of the mechanism of the mobilisation of armour rock and the pattern of the deformation

Each category will be described in the following sections.

The applied studies are also summarised in Table 1. The table provides an overview of the studies applied in the review, how it is applied, and how data has been obtained from each study.

2.1 Quantitative studies of stability of armour rock

The first category focusing on the actual stability of the armour rock i.e. the initiation of motion of the armour rock. These studies have been conducted by observing the movements of the armour rock while the flow intensity has been increased in small steps. Each flow condition has been applied for a relatively short period of time, typically a few minutes. The benefit of this approach is that it provides a lot of data in a relative short period of time and a reliable set of data of the initiation of motion. However, the initiation of motion of the armour rock is not necessarily a good measure for the severity of the initiated motion.

For instance, Nielsen and Petersen (2019) reported that the motion of the armour rock increased gradually with increasing wave height in the case of waves only, without a clearly defined threshold for inducing severe damage. On the other hand, Nielsen and Petersen (2019) also reported that the initiation of motion by the horseshoe vortex was associated with severe damage to the armour layer in case of steady current.

A major key study in this category is the de Vos et al. (2011) which also provided significant data to the already mentioned Nielsen and Petersen (2019).

2.2 Quantitative studies of the size of deformation of the scour protection

As mentioned in the previous section, the studies of the initiation of motion of the armour rock does not provide quantification of the severity of the motion or deformation of the scour protection. However, the magnitude of the deformation of the scour protection is important information both to be able to evaluate if it is acceptable at all and also to design a scour protection that can accommodate the magnitude of the anticipated deformation. Several studies have looked at this over the past two decades with a fairly consistent methodology: The bathymetry of the scour

Table 1: Overview of the different studies applied in this review. The column "Deformation, S, obtained" gives the origin of the deformation data, if a reference is given the deformation is taken directly from that reference. The quantities D_p, D_{50}, h, H_{m0}, T_p, and V are applied as provided in the in the source. Negative current velocity, V, shows that the current was opposing the waves, while "±" means the current direction was change during the test. All tests are flume tests, i.e. waves and current were either co-directional or opposing. Note, only data from tests applied in the analyses are included in the intervals, not all data is applied for all analysis. The ranges given for Nielsen and Petersen (2019) covers only relevant new data presented in Nielsen and Petersen (2019).

Author(s)	Qual. analysis	Quan. analysis	Time scale analysis	Deformation, S, obtained	D_p [m]	D_{50} [mm]	h [m]	H_{m0} [cm]	T_p [s]	V [cm/s]
De Vos (2008)	Yes	Yes	No	Wu et al. (2020)	0.1	4.0	0.40	6.9-14.6	1.2-1.7	-14.2-23.0
Loosveldt and Vannieuwenhuyse (2012)	Yes	No	No	N/A	0.05-0.13	4.0-11.5	0.2-0.5	5.7-16.0	1.4-2.2	-28.0-31.0
Schendel et al. (2014)	No	No	Yes	N/A	1.0	12.0	500	70-130	8.0	N/A
Ferradosa (2018)	Yes	No	Yes	N/A	0.1	2.7-7.5	0.24-0.50	8.6-14.5	1.5	14.7-22.2
Schendel et al. (2018)	No	No	Yes	N/A	0.15	0.19	0.5	N/A	N/A	16.6-25.3
Nielsen and Petersen (2019)	Yes	Yes	No	N/A	4.0-20.0	0.18-23	10.0-80.0	N/A	N/A	6.2-126.3
Wu et al. (2020)	Yes	Yes	No	Wu et al. (2020)	0.3-0.6	6.7-13.5	0.9-1.8	18.8-44.3	2.0-2.9	-57.0-37.7
Chambel et al. (2023)	Yes	No	No	N/A	0.1	6.0	0.36	10.5-10.6	1.5	10-15
De Lemos et al. (2023)	Yes	Yes	Yes	De Lemos et al. (2023)	0.08	0.18	0.50	N/A	N/A	17.0-21.0
Deltares (2023*b*)	Yes	Yes	No	See Sec. 3.2.1	0.2	4.7-10.1	0.75	N/A	N/A	±33.0
Deltares (2024), Atlantic Basin	Yes	Yes	Yes	See Sec. 3.2.1	0.15-0.30	2.7-9.3	0.60-0.75	14.8-25.9	1.8-3.0	-39.9-39.8
Deltares (2024), Delta Flume	Yes	Yes	No	See Sec. 3.2.1	1.0	9.2-18.4	5.1-5.2	82.0-170.0	4.0-7.5	N/A

protection has been measured before, after, and, in some cases, during the exposure of a hydrodynamic forcing and the deformation has been found by subtracting the before and after bathymetries. The actual method for measuring the bathymetry of the scour protection has varied between different studies and the quality has generally increased over time due to the improved measuring techniques.

The two most applied methods are laser scans (e.g. de Vos et al. (2012), Ferradosa (2018), and Wu et al. (2020)) and photogrammetry (e.g. Nielsen et al. (2023), Chambel et al. (2023) and Deltares (2024) including Broekema et al. (2024)). Both methods provide high quality measurements, although it is noted that the data from de Vos et al. (2012) (raw data originated from de Vos (2008)) has a significant lower resolution than the more recent studies (personal communication with Dr. Minghao Wu). This is believed to be a result of the before mentioned general improvements of the measuring techniques.

The main difference between these studies is the approach to defining the required test duration. Two basic approaches have been applied: 1) a fixed test duration (typically defined by number of waves), and 2) test until equilibrium. The first approach was applied by de Vos et al. (2012), Schendel et al. (2014), Ferradosa (2018), Wu et al. (2020) among others, while the second was applied by Nielsen et al. (2023). Deltares (2024) applied a mix between the two methods, which gave the opportunity to apply numerous different test conditions, but, as discussed in Sec. 3.2.1, also gave some implications in the interpretation of the results.

The reason the approach of defining the test duration is an issue at all is that the deformation develops towards an equilibrium. The deformation of the scour protection is essential a clear water scour process, which is known to be very slow. De Lemos et al. (2023) reported more than a day of testing to reach equilibrium of a scour test even in a relatively small scale. First of all, this means that to run the test to a reasonable representation of an equilibrium can be very time consuming and secondly it may also provide an, at least at the first glance, misleading result as the time required to reach equilibrium in most cases will be much longer than the duration of a design storm. This has led to the approach of testing for a fixed duration equal to the duration of a typical design event. The benefit of this approach is that it gives more reasonable deformations for direct applications, but it provides little insight into the accumulated deformation caused by subsequent storms. In this respect it is important to keep in mind that the time scale of the deformation varies with the actual hydrodynamic conditions as discussed in Sec. 3.2 and 3.4. The dependency between the actual deformation, equilibrium deformation, and the time scale can be quantified using a time step model as demonstrated in Sec. 3.5.

2.3 Qualitative studies on the mechanism of the mobilisation of armour rock and the pattern of the deformation

The qualitative studies are another way of looking at the deformation of scour protections. While the quantitative studies aim at providing data that can be applied directly in for example a design process, the qualitative studies aim at improving the general understanding of the processes and what causes, in this case, the deformation of the scour protections.

Many of the studies include a qualitative analysis but with largely varying extent. De Vos et al. (2012) provides a brief overall description of the deformation pattern observed for waves alone, co-directional and opposing waves and current. Van Steijn et al. (2023) and Broekema et al. (2024) made an attempt to classify the deformation patterns visually and divide the tests into six classes (Class 1 to 6), where, roughly speaking, Class 1 is the mildest deformation and Class 6 is the most severe. However, the class definitions appear not to be easy applicable, at least in the way it is presented in the two articles. The classes was presented as function of MOB_{top} and KC_{tot}, which are the ratio of the undisturbed Shields number to the critical Shields number (θ/θ_{cr}) and the modified KC-number ($KC_{tot} = (u_m + V)T_p/D_p$), respectively. Where the wave induced maximum orbital velocity, u_m, is defined similar to the definition applied in this article as outlined in App. A, V is the depth averaged current velocity, T_p is the peak period for the wave condition, and D_p is the diameter of the monopile, see also Fig. 1. Furthermore, the KC-number is traditionally defined as $KC = u_m T_p/D_p$ and the Shields number, $\theta = \tau_{max}/(\rho_w g(s-1)D_{50})$ where τ_{max} is the maximum bed shear stress for u_m and V combined. The bed shear stress is, in this article, calculated using the parametrisation given in Roulund et al. (2016) (see App. B) assuming an undisturbed, infinity long bed with a roughness corresponding to the armour rock ($k_s = 2.5D_{50}$), and the wave period represented by T_p. Van Steijn et al. (2023) and Broekema et al. (2024) applied a slightly different method, but this has no impact on the overall conclusion, however, see also Sec. 4.3.1. The two parameters (MOB_{top} and KC_{tot}), however, do not separate the classes and all classes are largely overlapping with at least two other classes, in this representation. For instance, Class 6 is almost fully overlapping Class 2 to 5.

Nielsen et al. (2023) made an attempt to categorise the deformations of scour protection exposed to waves based on the categories defined by Umeda (2011). They found that the categories defined by Umeda (2011) could be applied

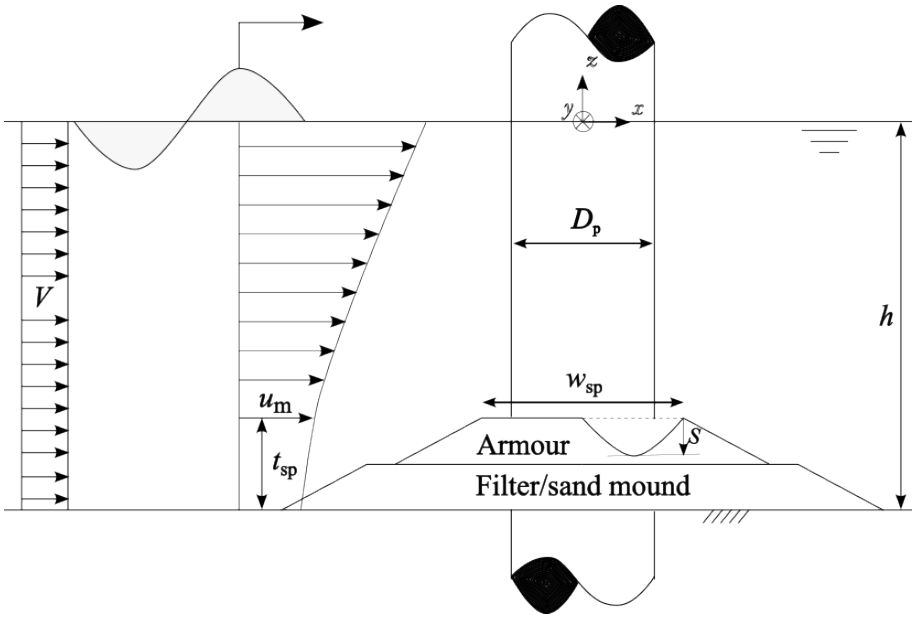

Figure 1: Definition sketch of the overall measures applied in this study. It should be noted that the data for the study comes from many sources with different setups. Many datasets do for example not include a filter layer and only a few setups include a sand mound.

to the deformation of scour protections by waves, but it was noted that the classification of the deformation patterns of the scour protections was somewhat difficult as important features of different deformation patterns would have appeared outside the area covered by the scour protection.

Nielsen and Petersen (2019) added descriptions of some of the mechanisms causing the deformation. That study had its main focus on steady current, where they found that the deformation was driven by two mechanisms, namely the lee-wake vortices and the horseshoe vortex. In the case of only waves the mechanisms was found to be contraction of streamlines combined with lee-wake vortex shedding in case of high KC-number (KC up to 14 was tested).

3 Re-analysis of the data

The data of the reviewed studies can basically be interpreted in two ways: qualitatively and quantitatively. Both methods of interpretation have been successfully applied on the data of Wu et al. (2020), including re-analysed de Vos (2008) data, and Deltares (2024) among others, while the data of Nielsen and Petersen (2019) only allows a quantitative interpretation in terms of thresholds for initiation of motion. On the other hand, Loosveldt and Vannieuwenhuyse (2012), Ferradosa (2018), and Chambel et al. (2023) only provides qualitative data (these studies also provide quantitative results in terms of damage numbers, see Eq. 9).

3.1 Qualitative interpretation

The present qualitative interpretation is based on a visual inspection and classification of deformation pattern of the scour protections tested by de Vos (2008), Loosveldt and Vannieuwenhuyse (2012), Ferradosa (2018), Wu et al. (2020), Chambel et al. (2023), de Lemos et al. (2023), and Deltares (2024) (both Deltares (2023a) and Deltares (2023b)). The benefit of this method is primarily that it is less sensitive to the duration of the tests compared to the quantitative interpretation. A recognisable deformation pattern will develop relatively fast, while the test duration required to reach an equilibrium of the deformation may be very long; the deformation is essentially a clear water scour process which is known to be very slow and can take days to reach equilibrium, even in small scale model tests, see e.g. de Lemos et al. (2023).

Two different classifications have been applied: one for waves alone and a simplified for waves, combined waves and current, and steady current. The classification of the deformation pattern for waves alone is based on the classification system presented by Umeda (2011) for clear water scour around a monopile exposed to regular waves. Umeda (2013) showed that the method could also be applied in case of irregular waves and Nielsen et al. (2023) showed that it was

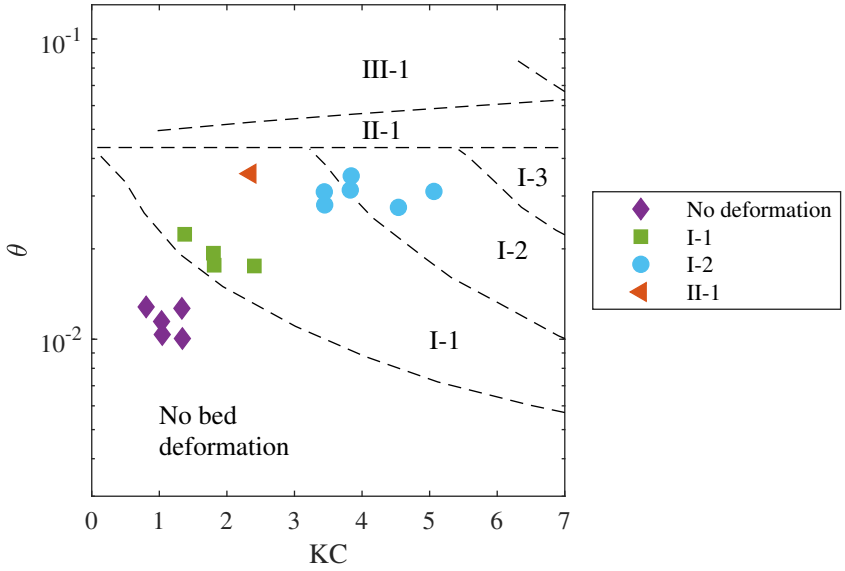

Figure 2: Wave results by Deltares (2024) (Atlantic and Delta flume tests) applied on the methodology by Umeda (2011). The categorization of the scour patterns is based on visual inspection of the measured scour protections. Scour protections with an extent of less than $3D_p$ or tests with breakthrough of the scour protection ($t_{sp} - D_{50} < S$) has been excluded.

applicable for deformations of scour protections around monopiles exposed to regular waves.

Umeda (2011) divided the scour pattern around a monopile into 11 categories depending on KC- and Shields number. These categories were then placed in groups: clear water (Group I), transitional scour (Group II), live-bed (Group III) as well as "No bed deformation". The groups were divided into subgroups; of relevance for the study are I-1 (Small scour), I-2 (Side scour), and II-1 (Detached scour). Furthermore, I-3 (Wake scour), III-1 (Vortex ripples), and III-2 (Truncated cone scour with vortex ripples) are within the ranges of KC and θ shown in Fig. 2 (III-2 are barely included). The Deltares (2024) study covers four of these categories and the observed patterns fits reasonable with the limits given by Umeda (2011), but the match is not perfect as seen in the figure. It must also be noted that the categorization is based on visual inspection of the measured scour protections provided by Deltares (2023a) and important features of some of the categories lay outside the scour protection area and therefore not included in the measurements, see also Nielsen et al. (2023) for details.

The classification by Umeda (2011) covers only waves alone and it was not possible to extend it to cover combined waves and current based on the available data. As the available data only cover a relatively small area around the monopile, some important features of the deformation pattern may develop outside the scour protection. This makes it impossible to develop a detailed classification, like the Umeda (2011) classification for wave alone, based on the scour protection data.

Nevertheless, it was possible to develop a simplified classification covering the full range from waves alone to steady current. This classification has three types of deformation (note, there is no direct link between this classification and the classification by Umeda (2011)):

- Type 1: No or small, mainly unstructured deformation.
- Type 2: Deformation at the side and downstream (relative to current direction) of the pile. Deposition between side and downstream deformation.
- Type 3: Deformation caused by horseshoe vortex or similar severe upstream deformation.

The benefit of this classification is that it is simple and easy to apply based on visual inspection. It is also roughly dividing the (u_{cw}, θ)-space (u_{cw} defined as $u_{cw} = |V|/(|V| + u_m)$) into:

1. Acceptable deformation (Type 1, S_{eq}/D_p typically smaller than 0.1).
2. Potentially critical deformation (Type 2, S_{eq}/D_p typically between 0.1 and 0.2)
3. Unacceptable deformation (Type 3, $S_{eq}/D_p > 0.2$)

Examples of the different types of deformations are shown in Fig. 3 and 4. All three types are shown in the two figures; examples of Type 1 are Panel H and M-O in Fig. 3, examples of Type 2 are Panel A, C, and E (both figures), and Type 3 is, among the examples, only seen in Fig. 4 in Panel F, K, and L.

It is observed in figs. 3 and 4 that there is a trend that the deformation will be more severe for both increasing u_{cw} and increasing Shields number. This is in line with previous studies; in the case of u_{cw} the same trend was reported by Sumer and Fredsøe (2001*b*) for $4 \leq KC \leq 26$ and de Lemos et al. (2023) for $KC \leq 7.5$, both under live-bed conditions. The Shields dependency is as reported by Baker (1986) (as presented by Melville and Sutherland (1988)) and de Lemos et al. (2023). Categorizing according to the three types and plotting the data as function of u_{cw} and θ shows that this is a consistent trend, see Fig. 5. As the three types of deformation is divided into three zones with relatively small overlaps.

It should be noted that the KC-number is not included as a parameter in Fig. 5. Detailed analyses have shown that the KC-number has little impact on the deformation in the tested range of $0.5 < KC < 5.5$, see Sec. 3.2.1. In that section it is shown that the deformation of the scour protection is practically independent of the KC-number in the range of 2 to 5.5 for a subset of tests from the Atlantic Basin test by Deltares (2024), that otherwise had similar conditions. The same was observed for combined waves and current by Nielsen and Petersen (2019) where no impact by the KC-number was found on the initiation of motion of armour rock in combined waves and current. Nielsen and Petersen (2019) reported for scour protections (critical conditions, transition from clear water to live-bed conditions). This corresponds to the results reported by Sumer and Fredsøe (2001*a*) for wave induced scour around a large vertical cylinder in live-bed conditions and waves. It was found that the scour process was governed by wave induced steady streaming ($KC < 2$) and was in a transition towards horseshoe vortex and vortex shedding induced scour in the range $2 \leq KC < 6$. The flow regimes will be the same in the case of clear water conditions as in live bed, as the transport mode is governed by the sediment or rock properties for given flow conditions (provided that the roughness of the sediment or rock will not change the main flow significantly). However, in live-bed conditions there will be an inflow of sediment from the surrounding seabed which may impact the size of the scour or deformation of a scour protection. Although Sumer and Fredsøe (2001*a*) did not report data in the transitional range ($2 \leq KC < 6$) but it is reasonable to assume that the relative scour will be constant in this range as the relative scour is the same at both sides of the range and hence the relative scour will be independent of KC in this range which was shown to be the case for u_{cw} around 0.35 by de Lemos et al. (2023). It is noted that Umeda (2011) found three to four distinctive clear water scour patterns in the range of $0 < KC < 6$, see Fig. 2; however, these are not found to have significantly different equilibrium scour depths, see Umeda (2011).

For low KC-numbers the diffraction of the waves can have an impact on the results. This is controlled by the ratio between pile size and wave length (D_p/L) and it is usually considered to have an impact when D_p/L become larger than around 0.1 to 0.2. For the present results D_p/L <0.08, so the impact by diffraction will be small, see e.g. Sumer and Fredsøe (2002).

Furthermore, Fig. 3 to 5 include data from tests where the deformation was larger than the thickness of the scour protection and hence some of the deformation has taken place in sand underneath the scour protection. Consequently, the magnitude of deformation shown in some of the plots in Fig. 3 and 4 is most likely larger than it would have been if the thickness of the tested scour protection had been sufficient to prevent breakthrough. However, there is no reason to believe that the deformation pattern would have been significantly different. Tests with an overall extent of the scour protection of less than $3D_p$ has been excluded as the primary deformation pattern tends to extent outside the scour protection in these cases making a classification questionable.

3.1.1 Remarks regarding initiation of rock motion

The mode of sediment and rock motion induced by flowing water is usually represented by the Shields number or the relative Shields number (MOB, the ratio of the Shields and critical Shields numbers). In this study the Shields number has been applied in favour of the relative Shields number, MOB_{top} (mobility number calculated at the top of the scour protection) for the following reasons. The relative Shields number is often introduced to compensate for the reduced critical Shields number in the transition between smooth and rough rock or sediment bed. However, the relatively large uncertainty of the Shields and critical Shields numbers will propagate to a considerable uncertainty when applying the relative Shields number. The author finds that this increased uncertainty will overshadow the benefits of the, in most cases, small correction due to reduced critical Shields number at the transition between smooth and rock bed. A numerical example can illustrate this. The MOB-scaling can be written as:

$$MOB = \frac{\theta_{model}}{\theta_{cr,model}} = \frac{\theta_{prototype}}{\theta_{cr,prototype}} \tag{1}$$

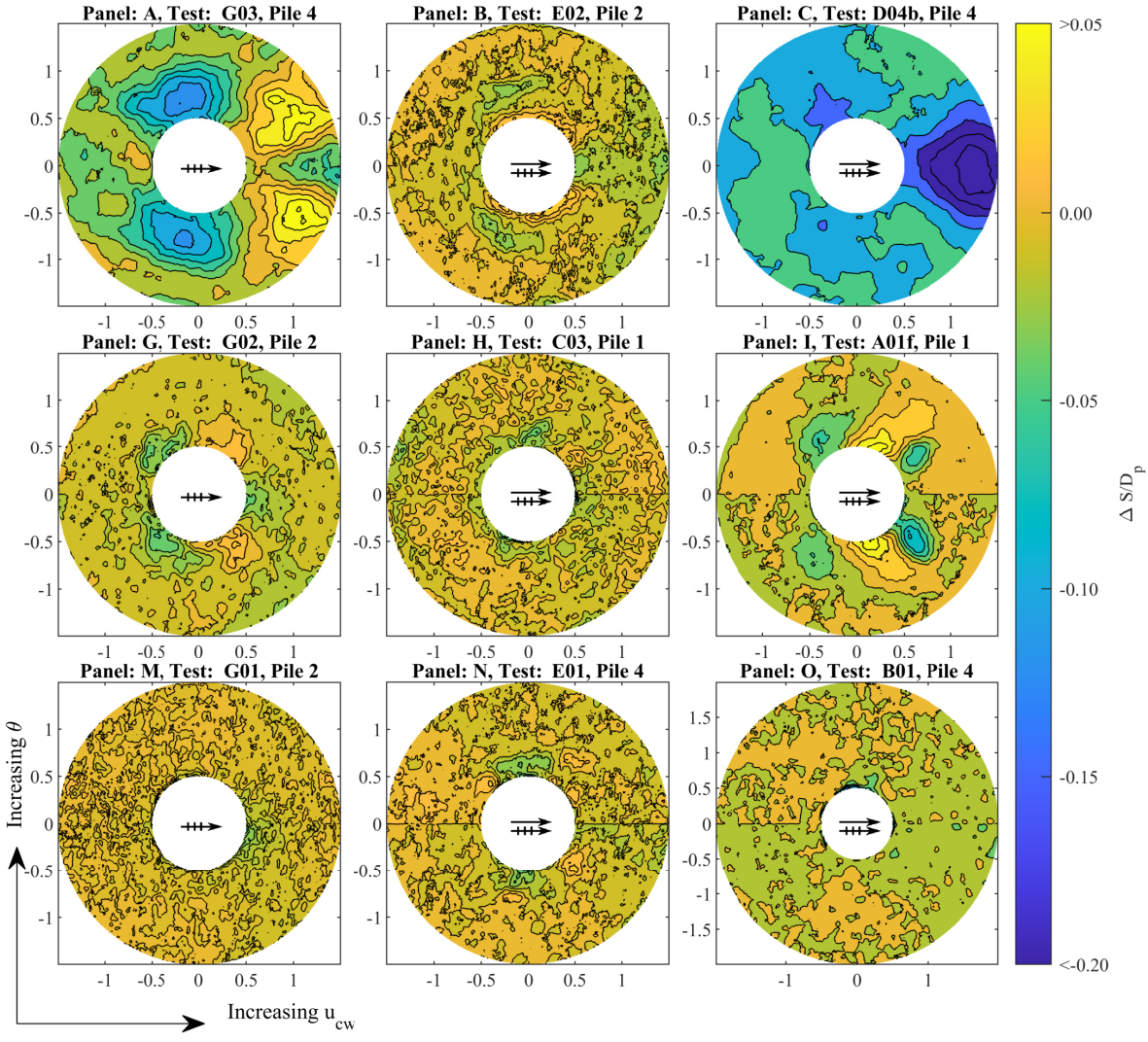

Figure 3: Examples of deformations of scour protections in the ranges of $0 \leq u_{cw} < 0.45$, $0.01 < \theta < 0.035$, and $KC < 5$. See Fig. 5 for details on wave-current ratio and Shields for each scour protection. The arrows in the middle of the plots indicating the direction of waves and current. It should be noted that deformation have exceeded armour layer thickness in some case (breakthrough). Data from Deltares (2024).

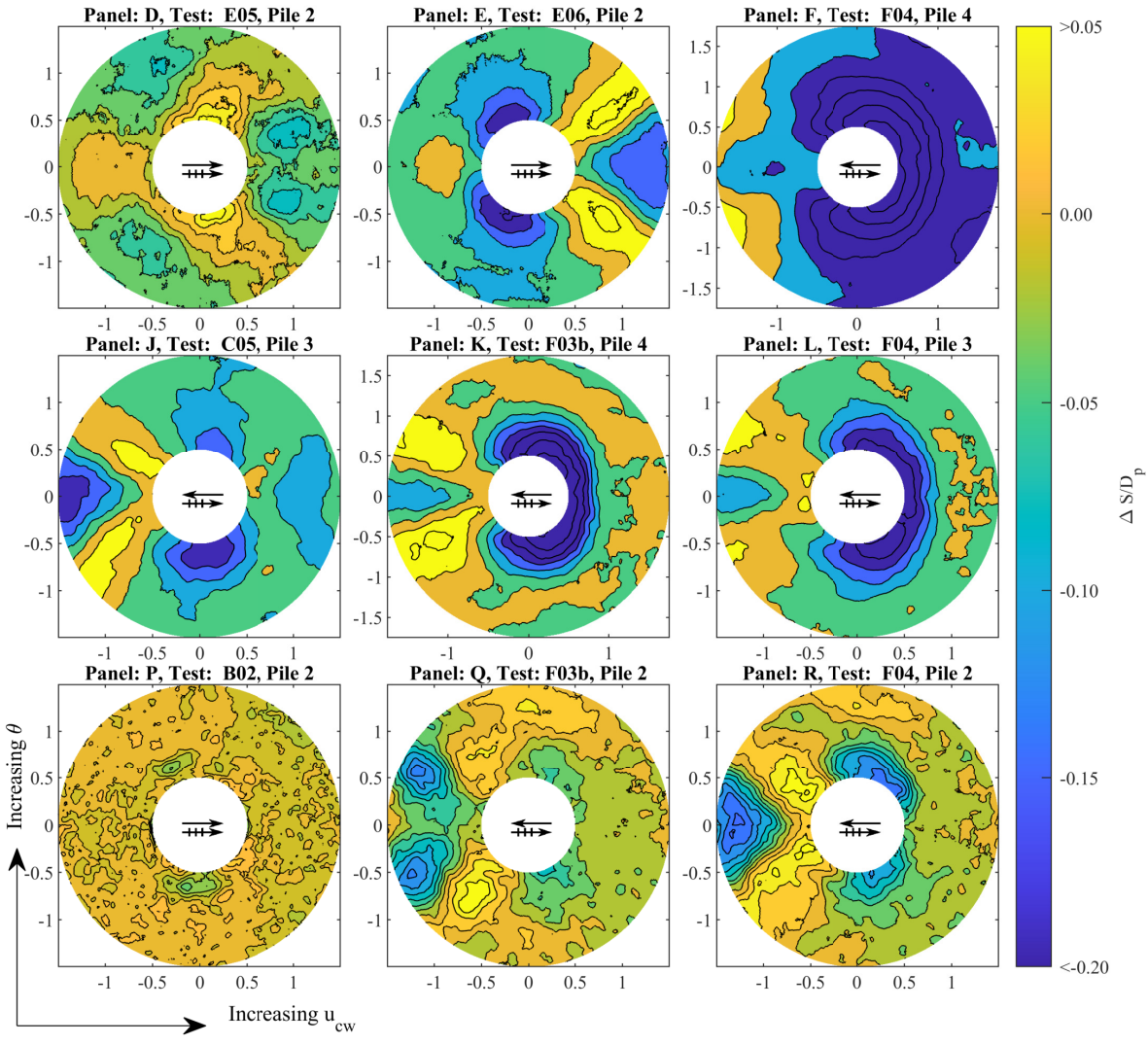

Figure 4: Examples of deformations of scour protections in the ranges of $0.4 < u_{cw} < 0.7$, $0.02 < \theta < 0.045$ and, $KC < 5$. See Fig. 5 for details on wave-current ratio and Shields for each scour protection. The arrows in the middle of the plots indicating the direction of waves and current. It should be noted that deformation have exceeded armour layer thickness in some case (breakthrough). Data from Deltares (2024).

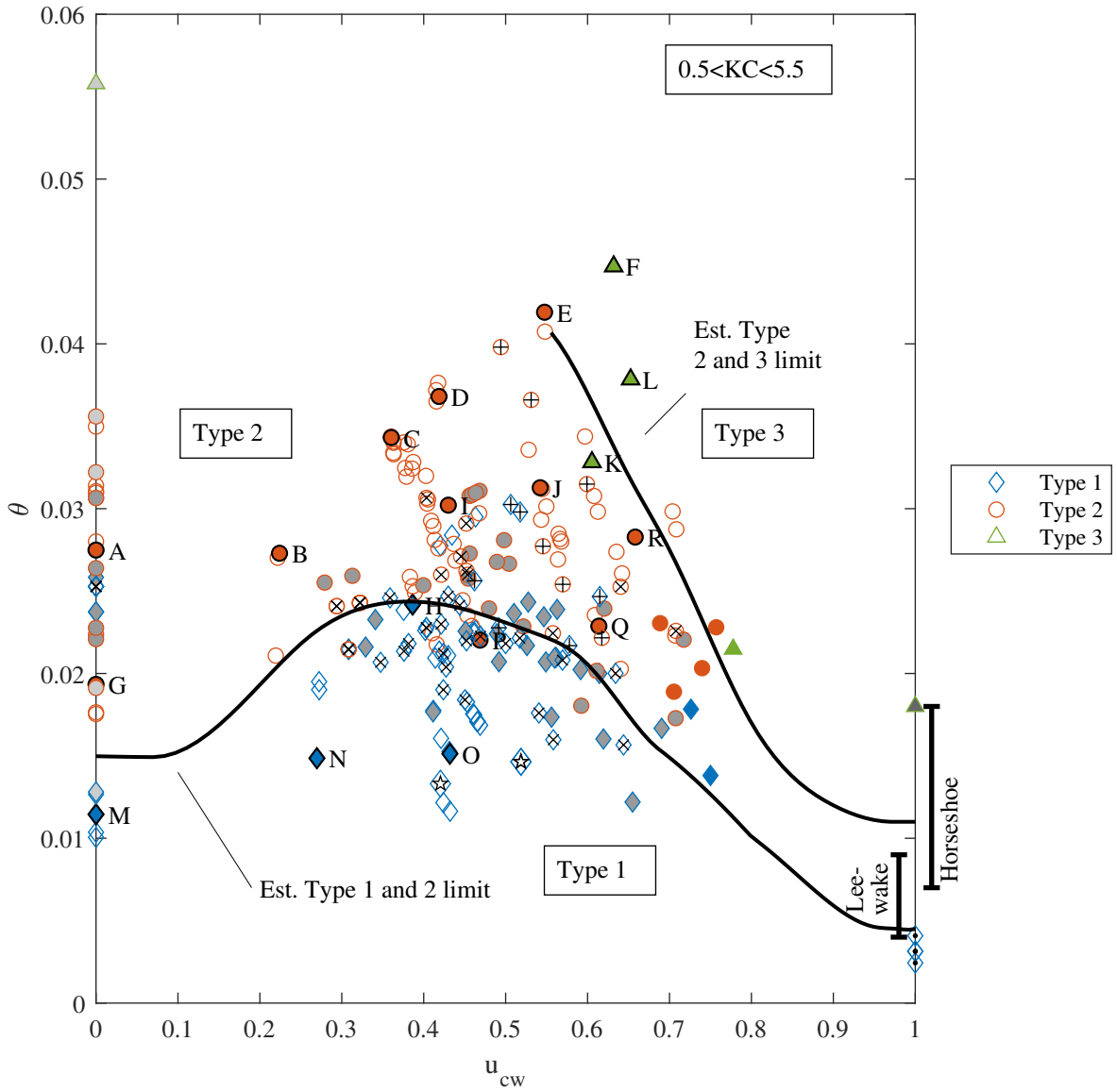

Figure 5: Deformation type of the scour protections as function of u_{cw} and Shields numbers; included data in the range $0.5 < KC < 5.5$. Three types of deformations, Types 1, 2 and 3 are indicated and the solid lines are the estimated border lines between these three types of deformation. Filled symbols with black edge show that the plot of the scour protection is shown in Fig. 3 and 4, the letters next to the data points refer to the relevant panels in the figures. Points without filling and filled points with black edges are from Atlantic Basin test by Deltares (2024), points with light grey filling ($u_{cw} = 0$) are from Delta Flume tests by Deltares (2024), points with darker grey filling ($0.0 \leq u_{cw} < 0.8$) are from de Vos (2008) (deformations types based on photo in Appendix VI, the deformation type was not identifiable for tests 24, 37, 38*, 39, 40, 41, and 51), filled points ($0.65 < u_{cw} < 0.8$) are from Wu et al. (2020), points with a black dot at $u_{cw} = 1$ are from the initial tests of Deltares (2023*b*) (part of Deltares (2024)), point with a plus ('+') are from Ferradosa (2018) (rock densities found via de Schoesitter et al. (2014)), points with a black 'x' are from Loosveldt and Vannieuwenhuyse (2012) (deformations types based on photo in Appendix E, the deformation type was not identifiable for test 35), points with a black star ('☆') are from Chambel et al. (2023), and the point with dark grey filling ($u_{cw} = 1$) is from de Lemos et al. (2023). Both u_{cw} and θ is based on u_m as representative for the wave motion. The bars at $u_{cw} = 1$ covers the ranges of initiation of motion by the lee-wake vortex and the horseshoe vortex based on Nielsen and Petersen (2019).

where θ_{model} is the Shields number and $\theta_{cr,model}$ is the critical Shields number the model scale rock, and $\theta_{prototype}$ and $\theta_{cr,prototype}$ are likewise for the prototype rock.

The propagated error of this when finding $\theta_{prototype}$ will be (assuming that the errors are dependent):

$$\frac{\Delta\theta_{prototype}}{\theta_{prototype}} = \frac{\Delta\theta_{cr,model}}{\theta_{cr,model}} + \frac{\Delta\theta_{model}}{\theta_{model}} + \frac{\Delta\theta_{cr,prototype}}{\theta_{cr,prototype}} \tag{2}$$

where $\Delta\theta$ is the estimated error of the relevant Shields number.

Similarly, by applying the definition of the Shields number ($\theta = \tau/(g\rho_w(s-1)D_{50})$) to Eq. 1, the relation between model scale and prototype rock size can be found:

$$D_{50,prototype} = \frac{\theta_{cr,model}}{\theta_{cr,prototype}} \frac{\tau_{prototype}\rho_{w,model}(s_{model}-1)}{\tau_{model}\rho_{w,prototype}(s_{prototype}-1)} D_{50,model} \tag{3}$$

where τ is the bed shear stress, ρ_w is the density of the water, and s is the relative density of the armour rock.

The error of the estimated $D_{50,prototype}$ can then be estimated, assuming that the estimated critical Shields numbers and the bed shear stresses are independent of each other:

$$\frac{\Delta D_{50,prototype}}{D_{50,prototype}} = \sqrt{\left(\frac{\Delta\theta_{cr,model}}{\theta_{cr,model}} + \frac{\Delta\theta_{cr,prototype}}{\theta_{cr,prototype}}\right)^2 + \left(\frac{\Delta\tau_{model}}{\tau_{model}} + \frac{\Delta\tau_{prototype}}{\tau_{prototype}}\right)^2} \tag{4}$$

This estimate is valid under the assumption that the errors of the bed shear stress and critical Shields numbers will dominate the total error as the of the density of water, relative density of the rock and the rock size are typically small and can be left out of the estimate of the propagated error.

The effect of the MOB and Shields scalings can then be compared based on Eqs. 2 and 4 as listed in Table 2. The "Direct Shields scaling" is based on $\theta_{cr,model}/\theta_{cr,prototype} = 1$, the "$MOB$ based on Soulsby and Whitehouse (1997)" is based on the parametrisation of the Shields curve by Soulsby and Whitehouse (1997):

$$\theta_{cr} = \frac{0.30}{1+1.2D_*} + 0.055(1-\exp(-0.020D_*)) \tag{5}$$

where $D_* = (g(s-1)/\nu^2)^{1/3}D_{50})$ and ν is the kinematic viscosity of water. The error of the critical Shields numbers is based on Figs 2 to 4 in the same article. This parametrisation by Soulsby and Whitehouse (1997) has been applied by many studies, including Wu et al. (2020) and Broekema et al. (2024). The "MOB based on Sumer and Fredsøe (2002)" is likewise based critical Shields numbers and corresponding errors found in Fig. 1.2 in the book.

The results in Table 2 shows that there may be an actual effect of applying the MOB-scaling. If the parametrisation by Soulsby and Whitehouse (1997) is applied the prototype median rock size will be around 80% of the rock size found using a direct Shields scaling. However, if the Shields curve presented in Sumer and Fredsøe (2002) is applied there is no effect other than an increased uncertainty of the result. The increased uncertainty is in fact the case for both Soulsby and Whitehouse (1997) and Sumer and Fredsøe (2002) Shields curves. Furthermore, it cannot be determined which of the two Shields curves there are predicting the actual critical Shields number best, but it can be said that the data presented in Soulsby and Whitehouse (1997) indicate that the Shields curve is different for regular waves and current. This is, at least partly, due to the definition of Shields in waves applying the maximum bed shear stress which only appears for very short time, too short to actually mobilise and move sediment and rocks. To actually move the rock, a duration of time is needed and that will in practice result in a higher maximum bed shear stress and critical Shields number, as also described by Soulsby and Whitehouse (1997). It should also be mentioned that, to the knowledge of the author, no data is available for critical Shields in irregular waves and combined irregular waves and current, so the MOB-scaling is basically based on an assumption that a certain Shields curve (typically based on steady current test and in some case also regular waves) are valid for combined current and irregular waves, where the waves are represented by statistical wave induced velocity, for example u_m as defined in App. A. However, as seen in Table 2, two different, but equally valid Shields curves can give very different results. To reduce the uncertainty as much as possible the Shields scaling will be applied. This also means that the results in this article are practically only valid for rough bed conditions.

It is noted that this only applies for the rock. Other scaling methods are applied for all other quantities like pile size, water depth, wave and current conditions, storm duration etc. Usually, the Froude scaling law is applied for these quantities, however, other parameters can be of relevance e.g. the Reynolds number. Both the Froude and Reynolds numbers has associated uncertainties, but these are relatively small as the quantities applied for these

Table 2: Examples of results and error propagation for a scaling of a model rock size of $D_{50} = 2.7$ mm (the smallest rock size applied, except for a few tests with sand, see Table 1) with a relative density $s = 2.65$ to typical prototype conditions (constant part of the Shields curve). For simplicity it is assumed that the relative density of the rock, s, and the water density, ρ_w, are the same in model and prototype scale.

Scaling	Direct Shields	MOB based on Soulsby and Whitehouse (1997)	MOB based on Sumer and Fredsøe (2002)
$D_{*,model}$	-	68	-
$Re_{cr,model}$	-	-	120
$\theta_{cr,model}$	-	0.045	0.045
$\theta_{cr,prototype}$	-	0.055	0.045
θ_{model} (est. see Sec. 3.2.6	0.02	0.02	0.02
$\theta_{prototype}$ (est. see Sec. 3.2.6	0.02	0.02	0.02
$\Delta\theta_{cr,model}$	-	0.03	0.015
$\Delta\theta_{cr,prototype}$	-	0.03	0.015
$\Delta\theta_{model}$	-	0.02	0.02
$\tau_{model}/\Delta\tau_{model}$ (based on Roulund et al. (2016))	-	0.2	0.2
$\tau_{prototype}/\Delta\tau_{prototype}$ (based on Roulund et al. (2016))	-	0.2	0.2
$\Delta\theta_{prototype}$ (Eq. 2)	$\pm$0.03	$\pm$0.04	$\pm$0.02
$\Delta D_{50,prototype}/D_{50,prototype}$ (Eq. 4)	$\pm$40%	$\pm$130%	$\pm$80%
Correction factor to Froude scaling of rock size ($\theta_{cr,model}/\theta_{cr,prototype}$)	1	0.8	1

numbers are relatively well-defined and usually with relatively small uncertainties, opposite the Shields number where the determination of the bed shear stress is in most cases relatively uncertain.

3.2 Quantitative interpretation

As already mentioned in Sec. 3.1 a quantitative analysis of the deformation of scour protections is much more sensitive to the test duration than the qualitative analysis presented in Sec. 3.1. Two different strategies are often applied to ensure consistent and comparable data: 1) Testing constant conditions until equilibrium or 2) testing of a fixed period of time (often defined as a specific number of waves). The strategy of testing to equilibrium is common practice when testing scour in live-bed conditions, see e.g. Sumer et al. (2013) and de Lemos et al. (2023) among others, and it has also been applied for various scour protection tests, e.g. Nielsen et al. (2011, 2013, 2015) and Petersen et al. (2015) covering sinking of scour protections and edge scour. The method has only been consistently applied for armour rock stability in the study by Nielsen et al. (2023). Other studies such as de Vos (2008), de Vos et al. (2012), and Wu et al. (2020) have applied the strategy of testing for a fixed period of time.

It can be discussed which strategy is best. The duration required to reach equilibrium depends on the actual mobility of the armour rock, represented by the Shields number and indirectly the u_{cw} ratio. However, if moderate deformation is accepted the duration required to reach equilibrium will often be very long in the case of scour protection deformations and in many cases at least an order of magnitude longer than the expected duration of the design condition for practical applications. Hence, if this strategy is applied, the results will probably be the most consistent, but the deformation is likely to be large compared to what will be seen in practical applications. The strategy of a fixed test duration is likely to give somewhat more uncertainty in the results as the time scale of the deformation varies for different conditions, see Sec. 3.4. On the other hand, the magnitude of the deformations is likely to be more realistic provided that the test duration has been selected correctly relative to typical storm durations.

This means that for example the studies of Wu et al. (2020) and Nielsen et al. (2023) both can be expected to be internally consistent, but not necessarily directly comparable. It appears to be more complicated in the case of Deltares (2024). In this study the tests were conducted in test series where the hydrodynamic conditions were changed from test to test without rebuilding the scour protections (as in the case of Nielsen et al. (2023)), but without ensuring that equilibrium was reached after each test).

However, as demonstrated in Sec. 3.5 it is possible to setup a time step model based on equilibrium deformation and time scale of the deformation process to overcome the issue of test duration and achieved deformation.

The selection of data for the quantitative analysis from the different studies applied in the analysis is discussed in detail in the following sections. Note, only studies where the maximum equilibrium deformation, S_{eq}/D_p, is available is considered.

3.2.1 Selection of data from Deltares (2024) in Atlantic Basin, Deltares

As mentioned in the previous section, the data in Deltares (2024) obtained from tests with varying test conditions applied for durations not always long enough to reach equilibrium of the deformation process. This has resulted in a large dataset with multiple wave and current conditions, but with the drawback that not all the tests can be directly compared. Two tests with similar test conditions but in different test series can have significantly different sizes of the deformation of the scour protection as the conditions of the previous tests in the two test series have been very different and not reached equilibrium, at least in one of the cases. It is described, in the following how comparable tests has been identified for the further analyses.

The first step was an analysis of Test Series A. The test series included six tests with practically constant test conditions (Test A01a to A01f), which gives an indication of whether the equilibrium was reached. It should be noted that the test series, as all the test series in the Deltares (2024) Atlantic Basin tests, included four individual piles with scour protections, see Deltares (2023*a*) for details.

The development of the maximum observed deformation over the duration of the tests of the four scour protections are shown in Fig. 6. As seen in the figure, the deformation around Pile 2 and 3 seems to have reached equilibrium after around 2 to 2.5 hours, but the deformation around Pile 1 and 4 continues to develop and it not possible from this information to determine if the deformation has reached equilibrium at the end of the test.

It should, however, be noted that the deformation may remain stable adjacent to the pile or even back-filling while developing further away as seen in Fig. 7. This is also the case for Pile 1 and 4 in Test A01e to A01f, see Fig. 6 where the largest deformation takes place away from the pile (fully drawn lines), while the deformation adjacent to the piles is more or less constant (dashed lines). This also means that additional care should be taken before the data

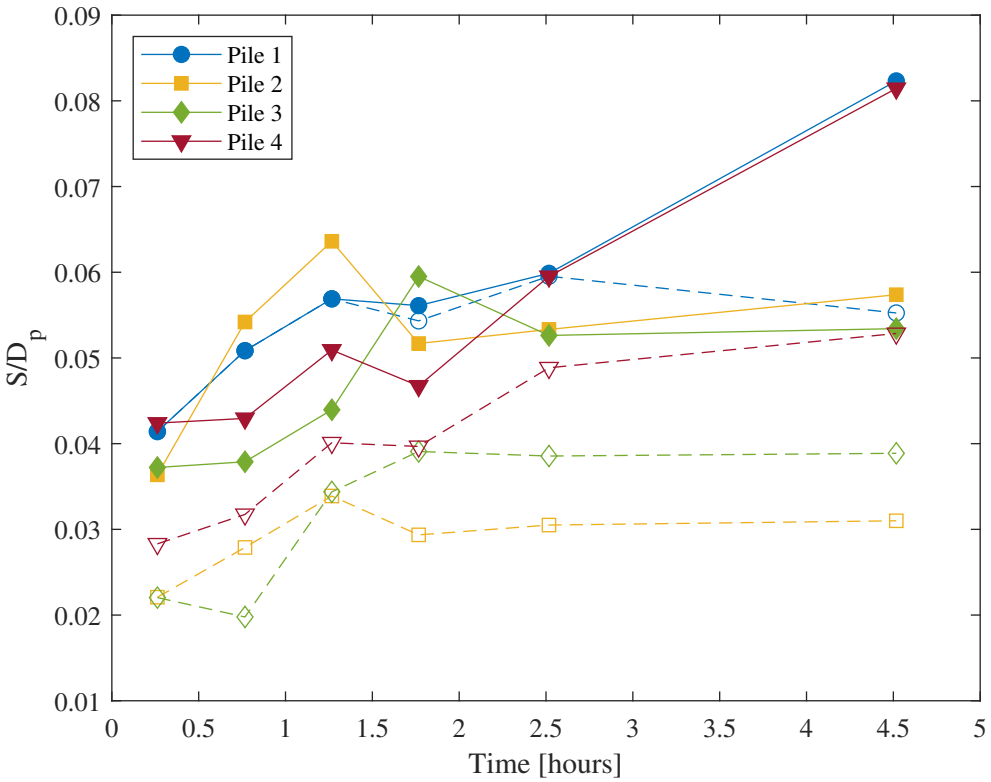

Figure 6: Relative deformation in the armour layer as function of the duration of the test series for Test Series A01a to A01f. The fully drawn lines and filled symbols are the maximum scour within $1.0D_p$ from pile centre while the dashed lines and open symbols are the maximum scour within $0.55D_p + 2D_{50}$ from the centre of the pile (adjacent to the pile). Data from Deltares (2024)

is applied. Diagrams are provided in Appendix F in Deltares (2023*a*) showing the development of the deformation adjacent to the pile with a high temporal resolution, but as shown in this paragraph it may not give a correct picture of the deformation development.

Given the test methodology applied for Deltares (2024) the realistic analysis of the data will have to focus on a equilibrium strategy. An attempt to determine deformation at a fixed duration is simply not found feasible given the varying test durations and accumulative deformations covering different test conditions. In order to find the tests, there are likely to be at equilibrium the relative deformation, S/D_p, was plotted as function of two relevant parameters: accumulated test duration, Σt and Shields number, θ, as seen in Fig. 8. The accumulated test duration is individual for each test series and is accumulated duration of the present and previous tests.

The upper panel of Fig. 8 shows the relative deformation as function of accumulated test duration. The deformation is generally increasing for increasing accumulated test duration, this is an indication that equilibrium is only reached at the end of each time series, but it can also be caused by the fact that most of the time series had increasingly severe conditions and hence expected larger deformations. Furthermore, a more detailed inspection of the results shows that in the case of Type 1 deformation, the relative deformation remains below 0.1, where in several cases the equilibrium is reached after a short duration of less than a couple of hours.

The lower panel (relative deformation as function of Shields number) shows a similar tendency with increasing deformation for increasing Shields number, so it is reasonable to conclude that there is a dependency of the Shields number on the deformation, which is also seen in Fig. 10.

Based on Fig. 8 it can be concluded that for the Deltares (2024) Atlantic Basin data the:

- Deformations depends on the Shields number.
- Reported deformations are representative for the equilibrium deformation in case of Type 1 deformations.
- Measured deformations appears representative of equilibrium scour when the accumulated test duration exceeds 6.5 h in case of Type 2 and 3 deformations.

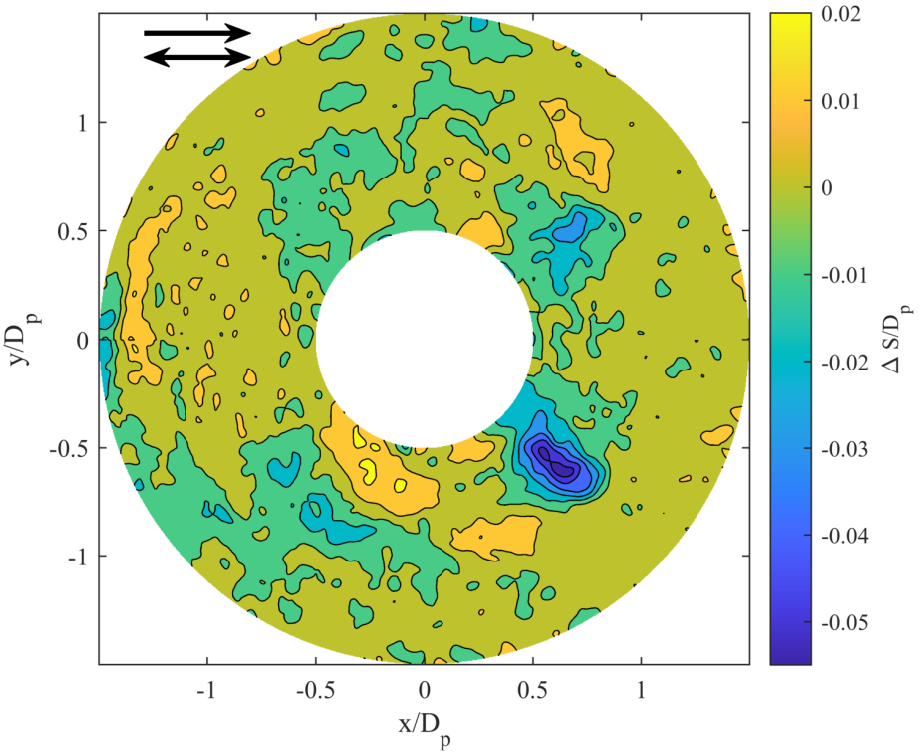

Figure 7: Difference in bathymetry of the scour protection between Test A01f and A01e for Pile 1. Data from Deltares (2024)

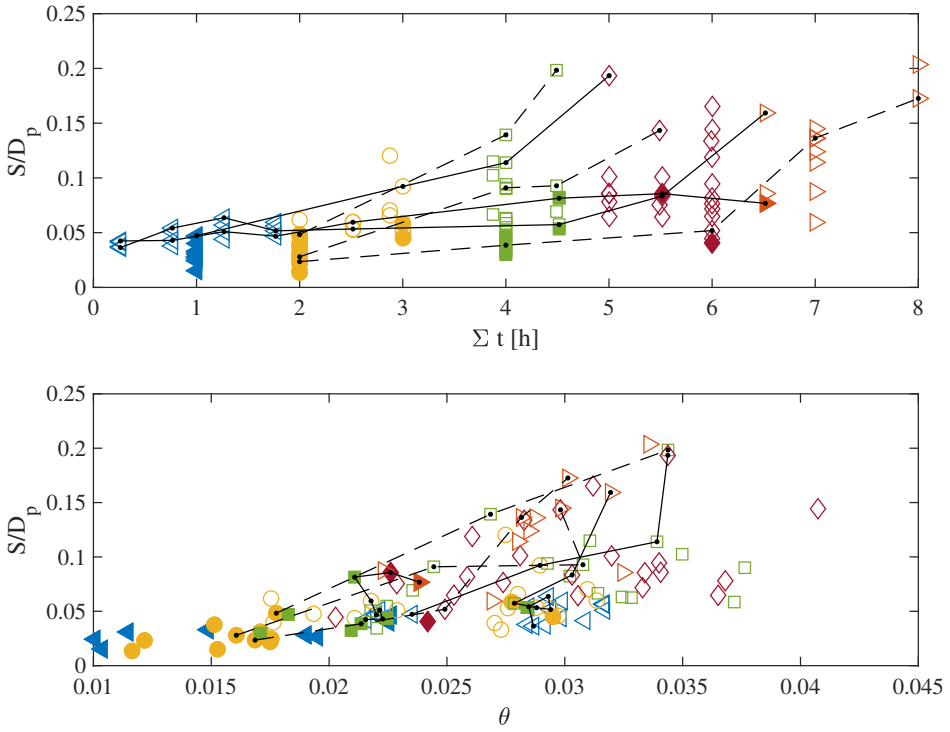

Figure 8: The relative deformation, S/D_p, as function of accumulated duration, Σt and θ. Filled symbols are Type 1 deformation pattern and the lines connects tests of representative test series. Test with scour protection extent less than $3D_p$ are excluded, as edge scour might have a major impact on the stability of the scour protection. Likewise, individual tests with $(S > t_{sp} - D_{50})$ are excluded as this large deformation indicates breakthrough of the armour layer and scouring of the much more erodible underlaying sand or filter material. Data from Deltares (2024).

The requirements to the accumulated test duration to have a reasonable representation of the equilibrium situation is to some degree uncertain for Type 2 and 3 deformations. The accumulated test duration is just an indication of the required duration to reach equilibrium, and the same accumulated test duration may cover a broad range of conditions. Hence, the deformations for two scour protections and piles of the same design may, after a certain accumulated test duration, be very different if the hydrodynamic conditions have been different and the time to reach equilibrium may be very different for the two cases. This means that equilibrium may be reached after relatively short time for some test series while it will take much longer for others. There may also be situations where a certain test reached equilibrium, while the following in the same test series did not. However, to find and remove these cases from the data set will require a manual assessment of each test which will almost certainly be arbitrary, at least to some extent. To avoid arbitrary sorting of the data it was decided to apply constant threshold for the accumulated test duration. This threshold was set to 6.5 hours, which is found to be a reasonable compromise between avoiding too many underdeveloped tests and keeping as much reliable data as possible. For accumulated test durations of less than 6.5 hours there appears to be a relative high spreading of the deformations for higher Shields number ($\theta > 0.025$); this is much less pronounced for accumulated test durations of at least 6.5 hours, where most of the data points at the upper part of the data cloud, indicating that the results are closer to equilibrium. Tests of Type 1 are included in the dataset independent of the accumulated test duration. Furthermore, data from Deltares (2024) Test A01a to A01e has been removed as these are represented by Test A01f.

In addition to the Shields number, the deformation is sometimes described as dependent on the KC-number, see for example Broekema et al. (2024) or the u_{cw}-ratio, see Nielsen and Petersen (2019). The dependency on the u_{cw}-ratio will be discussed in Sec. 3.2.6 while the effect of the KC-number will be considered here. Fig. 9 shows the same data as in Fig. 8 but with the relative deformation as function of Shields and KC-number. Most of the deformation intervals lays within a narrow range of KC-numbers, for example, all equilibrium tests within the deformation range of $S_{eq}/D_p < 0.05$ lay in the interval $1 < KC < 2.5$, which make it difficult to determine the dependency on the KC-number. The deformation range $0.15 \leq S_{eq}/D_p < 0.21$ is also in a narrow range of KC-numbers ($2.7 < KC < 4.0$), while $0.10 \leq S_{eq}/D_p < 0.15$ covers a broader range of $1.6 < KC < 3.4$, but these tests covers a relative larger range of u_{cw}-number ($0.56 < u_{cw} < 0.71$) which in it self can cause a larger difference in relative deformation, see Fig. 11. However, a subset of the range $0.05 \leq S_{eq}/D_p < 0.10$ provides a broad range of KC-numbers ($2.1 < KC < 5.4$) and a reasonable narrow range of u_{cw} ($0.37 < u_{cw} < 0.44$); the data points of this subset of tests are marked as filled sqaures.

The only trend of these data points appears to be that they are within the same range of Shields numbers and hence independent of the KC-number. This is also illustrated by the best linear fit to the data point shown as a thick black line that is almost horizontal. The thin black lines are the one standard deviation confidence interval. This shows that the deformation is practically independent of the KC-number in case of combined waves and current in the studied range of KC ($1.5 < KC < 5.5$) and u_{cw} around 0.4, which is inline with the finding for waves alone shown in Fig. 10 and the finding for combined waves and current by Nielsen and Petersen (2019). Based on this it is reasonable to conclude that the results can be considered independent of the KC-number for $KC < 5.5$ and clear water conditions. Furthermore, the deformation intervals $0.10 \leq S_q/D_p < 0.15$ and $0.15 \leq S_q/D_p < 0.21$ shows the same trend and as mentioned before the range of KC-numbers for $S_{eq}/D_p < 0.05$ is too narrow to be conclusive.

It is noted that Deltares (2024) provided bathymetrical measurements of the scour protections. The deformation, S, was taken as the maximum deformation within $0.8D_p$ from the pile centre. The exclusion of data further away than $0.8D_p$ from the pile centre was made to avoid effect of edge scour. The distance of $0.8D_p$ is based on experience and visual inspection of the plotted bathymetries, see e.g. Appendix E in Deltares (2023a), where it is seen that the deformation caused by the pile takes place within this zone, see also Fig. 7.

The selected data has grain Reynolds numbers in the range $75 < Re < 635$. This means that the scour protections were hydraulic rough and that the critical Shields numbers were at the constant part of the Shields curve as practically all full scale structures. The grain Reynolds number is defined as $Re = U_f D_{50}/\nu$ where U_f is the friction velocity based on the bed shear stress found using the parametrisation given in Roulund et al. (2016) ($U_f = \sqrt{\tau/\rho}$), and ν is the kinematic viscosity of the water.

3.2.2 Selection of data from Deltares (2024), Delta Flume

The duration of both the individual test and accumulated test series of the Deltares (2024) Delta Flume test series was shorter than the tests in the Atlantic Basin. The duration of the individual tests varied from a little more than 30 min to around 50 min and the accumulated duration of the two test series was a little less than 2 and 3 hours for Test Series A and B, respectively. In this context it should also be recalled that the wave peak period in the Delta Flume was two to three times longer than in the Atlantic Basin and consequently the scour protections in the Delta Flume

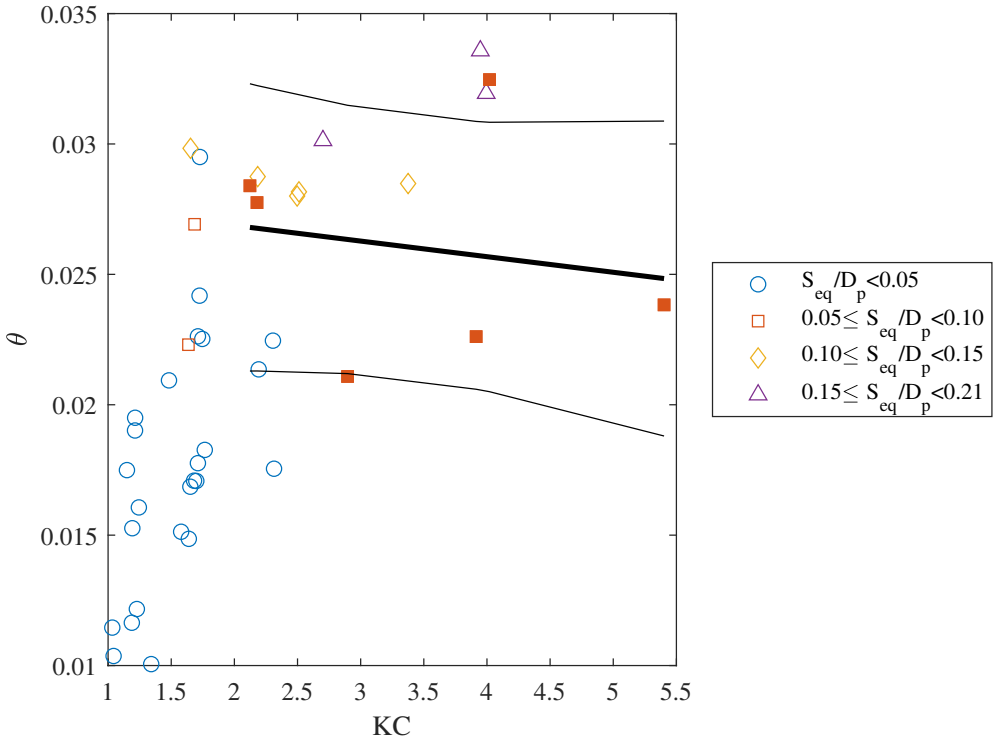

Figure 9: The relative equilibrium deformation, S_{eq}/D_p, of the data in Fig. 8 found to be equilibrium but as function of the Shields and KC-numbers. A subset of these tests is further highlighted with filled markers. These tests lays in the range of $0.37 < u_{cw} < 0.44$ so the influence of the u_{cw}-ratio on the deformation can be considered small. The thick black line is the best linear fit of these points, and the thinner black lines indicate one standard deviation confidence. Data from Deltares (2024).

tests have been exposed to significantly fewer waves than in the Atlantic Basin tests. However, Test A01 and B00 resulted in Type 1 scour and based on the analysis of the Atlantic Basin results (Sec. 3.2.1) it is reasonable to assume that the deformations measured after these tests are representative for the equilibrium. Of the remain five tests, two (A03 and B03) were discarded due to breakthrough of the armour layer by the deformation, the three last tests were kept in the quantitative analysis as they seem to follow the trend of previous tests (see Fig. 10). Furthermore, the analysis of the time scale of the deformation process (Sec. 3.4) indicates that the time scale of waves may be shorter than deformation by combined waves and current, perhaps as much as a factor of ten, although this is rather uncertain. Nevertheless, it is found plausible that the results are representative of the equilibrium scour to the same degree as the Atlantic basin tests.

Inline with the findings by Nielsen et al. (2023), the deformation appears to increase linearly with the Shields number for irregular waves. The trend line in Fig. 10 is the best straight line through the data by Deltares (2024) (Atlantic Basin and Delta Flume) and Umeda (2013) for Shields numbers up to 0.04:

$$\frac{S_{eq}}{D_p} = 3.3\theta - 0.008 \tag{6}$$

It should be noted that the transition between clear water and live-bed in Fig. 10 tends to take place at a higher Shields number ($\theta = 0.05$ to 0.06) than the critical Shields number given by the Shields curve for current and rough bed ($\theta_{cr} = 0.03$ to 0.06), see e.g. Sumer and Fredsøe (2002). Similar effects have been observed when testing for the critical Shields number in case of oscillatory motion, see e.g. Rance and Warren (1969); Willis (1978) as presented by Soulsby and Whitehouse (1997). The same effect was reported by Vithana (2013) and can be seen in the data by Sumer et al. (2001); Dixen et al. (2008) (only tests with particles of similar size as the surrounding rocks are to be considered), all studies of initiation of motion of single particles among otherwise stable particles. This effect is usually attributed to the definition of the Shields number in waves based on the near bed horizontal wave velocity amplitude; although the bed shear stress is large enough to mobilise the material, it is only large enough for a very short period of time for each wave cycle; not long enough to mobilise and transport a grain to a new position, hence a higher bed shear stress is required to actually initiate motion of the material.

The selected data has grain Reynolds numbers in the range $400 < Re < 1300$. As for the Atlantic Basin tests (Sec.

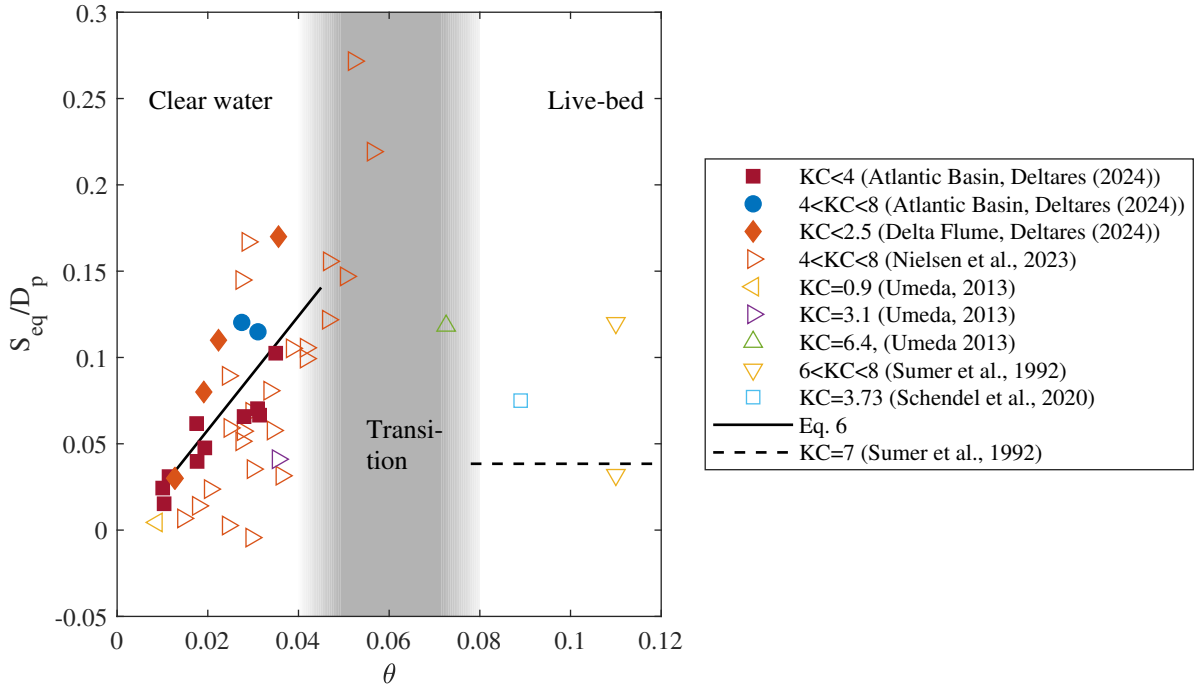

Figure 10: Clear water scour and deformation of scour protections as function of the Shields number in case of waves alone. Note, tests with $KC > 8$ presented in Sumer et al. (1992); Umeda (2013); Schendel et al. (2020); Nielsen et al. (2023) are left out for clarity; this is also the case for tests from Sumer et al. (1992) with relative scour depth presented as '~ 0', as well as tests with $\theta > 0.12$.

3.2.1), this means that the scour protections were hydraulic rough and that the critical Shields numbers were at the constant part of the Shields curve as practically all full scale structures.

3.2.3 Selection of data from Wu et al. (2020)

The Wu et al. (2020) tests including reanalysed results from de Vos (2008). These tests were conducted with 3000 waves ($3000T_p$) and according to de Vos (2008) this is an insufficient test duration to reach equilibrium, and the deformation was reported to be up to around 1.25 times larger after 5000 waves compared to 3000 waves. Furthermore, equilibrium was probably not reached even after 5000 waves. The tests by Loosveldt and Vannieuwenhuyse (2012) were conducted under similar conditions and gave similar results for up to 9000 waves. The deformation appears to be developing even after 9000 waves, but slowly, and the damage number was again around 1.25 time higher at 9000 waves compared to 3000 waves.

Wu et al. (2020) found the deformation directly by subtracting the before and after bathymetrical measurements of the scour protections (personal communication with Dr. Minghao Wu), while a moving average disk filter was applied for Deltares (2024). The moving average disk filter will remove the most extreme elements of the bathymetrical measurements, for example holes between rocks and a single rock at the top of the scour protection, which can appear as very large deformation when two bathymetrical measurements are subtracted. This also means that Wu et al. (2020) including the reanalysed data from de Vos (2008) will include some extreme deformations that have been filtered out of the Deltares (2024) data, see Deltares (2023*a*) for details. The effect of applying the unfiltered data can be as much as $S/D_p = 0.08$ (or $2D_{50}/D_p$), but in most cases around $0.05D_p$ or less. However, the underestimation due to the short test duration is estimated to be around 30% or 0.03 for a typical reported deformation of $0.1D_p$. Comparing these numbers shows that the Wu et al. (2020) data is likely to be comparable to the deformations found in the Deltares (2024) measurements, although Wu et al. (2020) might find slightly larger deformations for the same condition.

Based on the discussion in the previous two paragraphs, it was decided to include these results as: 1) the bias of the deformation due to the relatively short test duration is assumed to be similar to the bias of the other datasets, and 2) the methodology to find the deformation was slightly different and will result in a larger maximum deformation.

The selected data has grain Reynolds numbers in the range $300 < Re < 960$ for the original Wu et al. (2020) data and $105 < Re < 185$ for reanalysed data from de Vos (2008). So, also in this case the scour protections was hydraulic rough and the critical Shields numbers were at the constant part of the Shields curve as practically all full

scale structures.

3.2.4 Selection of data from de Lemos et al. (2023)

Two data points from de Lemos et al. (2023) has been included. De Lemos et al. (2023) studied clear waters scour in current and the tests were therefore conducted in fine sand ($d_{50} = 0.18$ mm) where the scour appeared as a conical shape hole. The scour development was measured with a high temporal resolution so the equilibrium scour, and time scale of the process could be found to an accuracy at least as good as for the other datasets.

The grain Reynolds numbers for these two data points are much lower than for the other studies as they were conducted in sand. The Reynolds numbers were 1 and 2, which corresponds to a smooth bed and maybe also a higher critical Shields number than the remainder of the tests. However, Eq. 5 gives a critical Shields number of $\theta_{cr} = 0.06$ while de Lemos et al. (2023) reported $\theta_{cr} = 0.035$ based on experimentally determined critical velocity. Both values are within the scatter of the Shields curve for current presented in Soulsby and Whitehouse (1997) ($0.03 < \theta_{cr} < 0.1$) and also in the case of rough bed where the scatter spans approximately ($0.02 < \theta_{cr} < 0.07$), so the results can be compared with other results considered, based on the Shields number.

3.2.5 Selection of data from Deltares (2023*b*) (part of Deltares (2024))

Four points from the test campaign on flexibility of loose rock scour protection Deltares (2023*b*), which is a part of Deltares (2024), is included as well. These points originate from the initial tidal current tests, intended to erode a sill of sand to form a falling apron, however, the results are found to be useful in this study as well. The scour protections have been exposed to 12 or 18 hours of constant current speed, but the direction was changes 180° every hour. Given the small deformation, this is found to be enough to reach equilibrium.

The selected data has grain Reynolds numbers in the range $95 < Re < 230$. Which is within the rough bed regime.

3.2.6 Deformation in combined waves and current

For live bed scour the equilibrium scour for combined waves and current is often presented as a function of u_{cw} and KC, where the latter appears as contour lines in the plot, see e.g. Sumer and Fredsøe (2001*b*). Wu et al. (2020) attempted to present the deformation of the scour protections in the same way, but without success. This is because the deformation is essentially a clear water scour process, and the Shields number has a major impact on the magnitude of the deformation. Nielsen and Petersen (2019) showed that initiation of motion of armour rock around a monopile is a function of Shields and u_{cw}-numbers, in case of low KC-numbers ($1 < KC < 10$). This is discussed in details in Sec. 3.2.1 (Fig. 9) Nielsen and Petersen (2019) furthermore showed, that a descriptive damage (categorized as "Low Damage", "Some Movements", and "Failure"), as defined by den Boon et al. (2004) and applied by de Vos (2008), de Vos et al. (2012) among others, could be described in the same way. As the deformation types can be organised in this way (Fig. 5) it is reasonable to plot the quantitative deformation in the same way. This is shown in Fig. 11 where the data selected according to the criteria established in Sec. 3.2.1 to 3.2.5, where it is seen that magnitude follows the expected trend of increasing deformation with increasing Shields and u_{cw}-numbers.

Nielsen and Petersen (2019) showed that the critical Shields number has a dependency on the rock size relative to the pile diameter (D_{50}/D_p) in case of current. This may also be the case for waves and combined waves and current. However, the tests applied have $D_{50}/D_p < 0.06$ where the critical Shields number was almost constant in case of current and plausible also for waves. Nielsen and Petersen (2019) did not present data on this for combined waves and current, but it is assumed that the critical Shields number was constant in this case as well and that deformation of the scour protection was unaffected by the rock-size-to-pile-diameter ratio within the applied interval $0.002 < D_{50}/D_p < 0.06$.

3.2.7 Remarks on current dominated conditions

Wu et al. (2020), Nielsen et al. (2023) and Deltares (2024) are all focusing on waves and combined waves and current. To cover the entire range from waves alone to steady current studies focusing on current must be included. Nielsen and Petersen (2019) presented a large dataset on initiation of motion of armour rock on scour protections around monopiles exposed to current as well as descriptions of the deformation mechanisms in both waves and steady current but did not quantify the deformation. However, the limits for the different motion from this dataset has been applied to establish the limits between Deformation Type 1, 2, and 3 in Fig. 5 and 11.

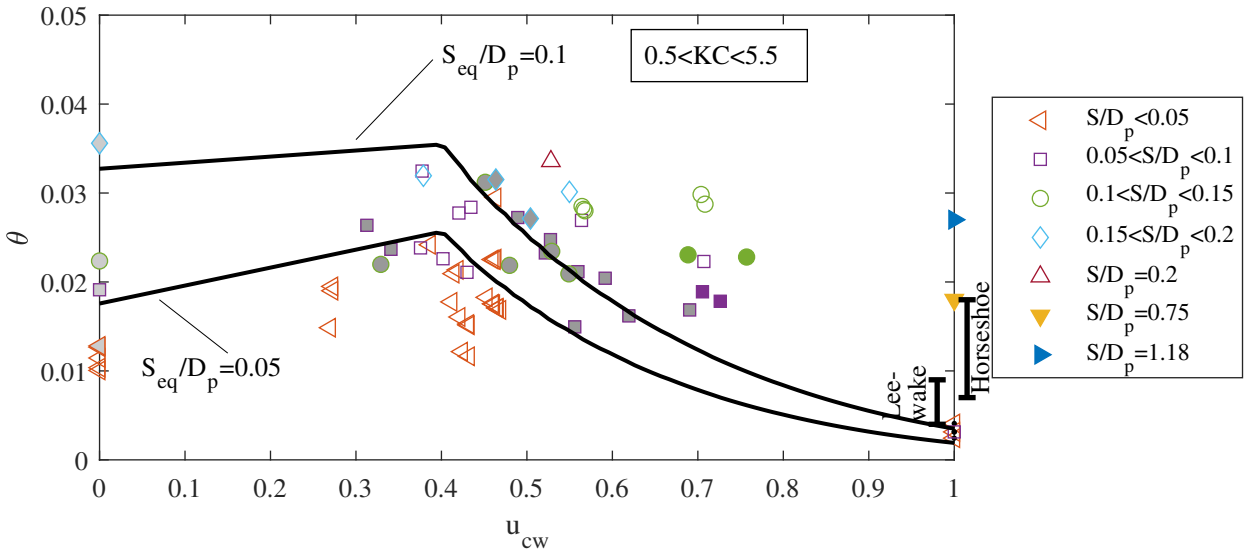

Figure 11: Maximum deformation relative to the pile diameter as function of the u_{cw} and θ (both based on u_m); included data in the range $0.5 < KC < 5.5$. Points without filling are from Atlantic Basin test by Deltares (2024), points with light grey filling ($u_{cw} = 0$) are from Delta Flume tests by Deltares (2024), points with darker grey filling ($0.3 < u_{cw} < 0.8$) are from de Vos (2008) as reanalysed by Wu et al. (2020), filled points ($0.65 < u_{cw} < 0.8$) are from Wu et al. (2020), points with a black dot at $u_{cw} = 1$ are from the initial tests of Deltares (2023*b*) (part of Deltares (2024)), and the points at $u_{cw} = 1$ are from de Lemos et al. (2023). The bars at $u_{cw} = 1$ cover the ranges of initiation of motion by the lee-wake vortex and the horseshoe vortex based on Nielsen and Petersen (2019). The trend lines are based on Eq. 7.

The deformation mechanism in waves was found to be very different from steady current, see Nielsen and Petersen (2019). In waves the deformation evolved gradually with increasingly larger waves (Shields number) without a sudden failure. This is also seen in Fig. 11 where the deformation of the scour protection increased gradually for increasing Shields number.

This is different from the steady current case as described by Nielsen and Petersen (2019). In the study it was found that the first motion of the rock appeared in the lee-wake of the monopile for Shields numbers around 0.005. The motion of the armour rock was, however, found to cause little or no accumulative damage to the scour protection as the lee-wake vortices tended to move the rock back and forth, rather than in a certain direction. This is in major contrast to the deformation caused by the horseshoe vortex, Shields number around 0.011, which causes a sudden mobilisation of the rock adjacent to the upstream side of the pile that removed all rock in the scour protection. Opposite the wave dominated situation where even relatively high Shields number will cause little deformation of the scour protection, it is reasonable to believe that the horseshoe vortex generated by current slightly above the critical velocity can cause a significant scour hole in the scour protection.

The deformation or scouring of the scour protection is basically a clear water scour process. Although there are no deformation tests of scour protections in current available, tests of clear water scour around monopiles can be used. Baker (1986) as presented in Melville and Sutherland (1988) provided equilibrium scour depths for different current speeds covering both clear water and live-bed conditions. The results show a rapid increase in the scour depth with increasing velocity in the clear water regime; these results were recently confirmed by de Lemos et al. (2023). It should here be noted that Yao et al. (2018) found the critical Shields number for initiation of scour around a monopile in current to be 0.016 (for a pile truncated at $5D_p$), somewhat higher than what was found by Nielsen and Petersen (2019).

It must be kept in mind that the consequence of exceeding the critical Shields number in current dominated conditions is much higher than in wave dominated conditions. A relatively small exceedance of the critical Shields number can result in an almost sudden destruction of the scour protection if scouring of the scour protection material by the horseshoe vortex is initiated, see Nielsen and Petersen (2019) for details. Furthermore, the deformation of the scour protection can be large, in some situations more than $S/D_p = 1$, see e.g. Fig. 11. It will in practice not be feasible to accommodate such large deformation in a scour protection as the required thickness of the scour protection will be around a pile diameter or more. Based on the current knowledge it is recommended to design scour protections in current dominated conditions stable in both upstream side (horseshoe vortex) and down-stream side (lee-wake vortices), i.e. the critical Shields number should be less than approximately 0.004. If motion of the rock in

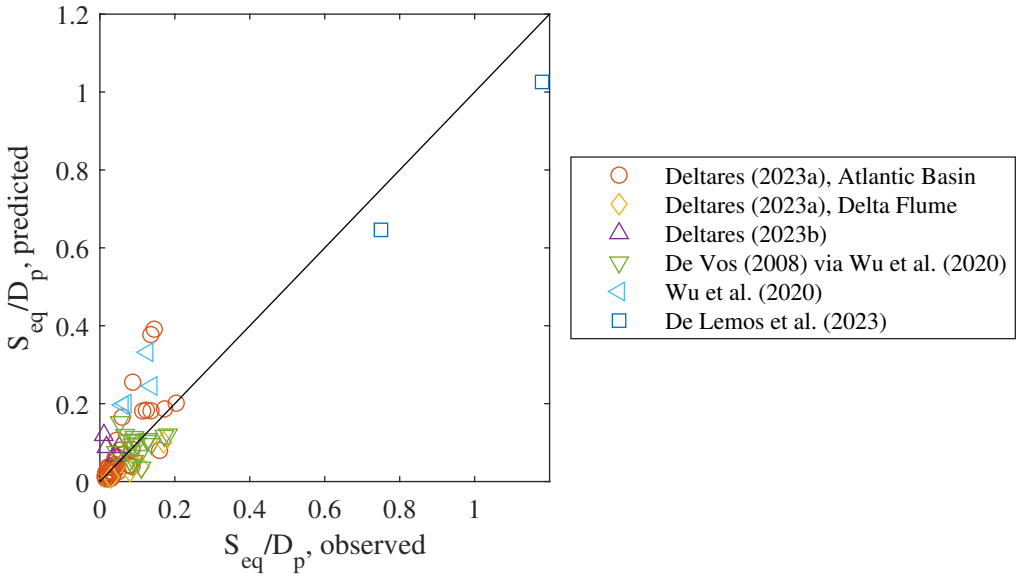

Figure 12: The performance of Eq. 7 on the data presented in Fig. 11. The correlation is 0.9 and RMSE=0.3.

the lee-wake is accepted the critical Shields number can be increased to around 0.008. It is under all circumstances important to consider the consequences of a failure as minor deviations from the design conditions may result in severe damage to the scour protection. It is also noted that the numbers given are without any safety factors.

3.3 Parametrisation of the scour protection deformation

Based on the data presented in Fig. 11 it is possible to develop a parametrisation that provide an estimate of the equilibrium relative deformation as function of the u_{cw} and Shields numbers. To do this, some assumptions must be made; little data is available for the most wave dominated situations (u_{cw} smaller than around 0.3), but the available data show a tendency that a certain deformation requires an increasing Shields number for increasing u_{cw} number. This is also in accordance with the trend seen for deformation type in Fig. 5 where more data is available for waves alone. However, the little data make it impossible to determine the actual size and shape of the variation except for waves alone where Eq. 6 provides an estimate of the equilibrium relative deformation as function of the Shields number for waves alone. This is applied and a linear relation is assumed between these deformations at $u_{cw} = 0$ and the current dominated conditions found for $u_{cw} \geq 0.4$. For $u_{cw} \geq 0.4$ the required Shields number to obtain a certain deformation tends to decrease with increasing u_{cw} number. This gives a basic set of formulas:

$$\frac{S_{eq}}{D_p} = \begin{cases} \frac{1}{0.4}(0.4 - u_{cw})(3.3\theta - 0.008) + \frac{1}{0.4} u_{cw} \left(a_1 a_2 \theta^{a_3} 0.4^{-\ln(a_2/\theta^{a_3})/\ln(0.4^{a_3})} \right) & \text{for } u_{cw} < 0.4 \\ a_1 a_2 \theta^{a_3} u_{cw}^{-\ln(a_2/\theta^{a_3})/\ln(0.4^{a_3})} & \text{for } u_{cw} \geq 0.4 \end{cases} \tag{7}$$

where $a_1 = 140$, $a_2 = 0.45$, and $a_3 = 1.14$ are fitting parameters determined by minimizing the root-mean-square-error (RMSE) for cases with $u_{cw} \geq 0.4$. The formula is valid for $0.5 < KC < 5.5$, $0.010 < \theta < 0.025$, and rough bed of the scour protection (in practice constant critical Shields number).

For the formula to provide the best possible estimate of the relative equilibrium deformation it is important to use the correct input parameters, see Sec. 4.3.1 for details. The procedure for calculating the parameters is outlined in App. C.

The performance of Eq. 7 on the data shown in Fig. 11 is plotted in Fig. 12. The correlation between the observed and predicted relative deformation is high, 0.9. However, this is also the case for the RMSE=0.3. Both numbers are strongly influenced by the two data points from de Lemos et al. (2023). Removing these two data points reduces the correlation to around 0.6 and the RMSE to around 0.05 but it will not influence the coefficients a_1 to a_3, significantly.

3.4 Time scale of the deformation

The time scale of the deformation is important for the assessment of the actual deformation during a storm, see also Sec. 5. The development of scour over time is often assumed to follow a exponential development, see e.g. Sumer

and Fredsøe (2002):

$$S(t) = S_{eq}\left(1 - \exp\left(-\frac{t}{T}\right)\right) \tag{8}$$

Where S_{eq} is the equilibrium scour depth, t is the time, and T is the time scale of the scour process. To apply this definition in practice requires that the time scale and equilibrium scour depth are known. The time scale can be estimated from physical model tests, but it requires, for it to be accurate, that the scour development is measured with a high frequency to capture the actual development. There is not much data of this kind available for deformation of scour protections, but Deltares (2024) provides a little in form of Test A01a to f, as already presented in Sec. 3.2.1 (Fig. 6). Furthermore, tests D04 to D04b Pile 2 and 4 (also from Deltares (2024)), data from Schendel et al. (2014), Schendel et al. (2018) (tests Uni01 to Uni03 and Tide 01), and de Lemos et al. (2023) (tests B1 and B2) were found to be applicable for estimating the time scale based on maximum deformation, S. Ferradosa (2018) provided time series with three to four steps that were found suitable for estimating the time scale, but these time series were based on the damage number, S_{3D}, originally introduced by de Vos (2008); de Vos et al. (2012) and defined as:

$$S_{3D} = \frac{V_s}{AD_{n,50}} \tag{9}$$

where V_s is the scoured volume, A is the subarea of which the measurement is taken, and $D_{n,50}$ is the nominal size of the median rock. It is noted that the area A is defined differently in different studies, see Ferradosa (2018) for the definition applied in that study.

It must be noticed that most of the time scales are estimated based on only three or four data points and in some cases the starting time has been estimated as well, as the data is taken from a longer test series. It is also noted that tests D04 to D04b Pile 2 and 4 (Deltares, 2024) had reasonable constant Shields and u_{cw} numbers, but the KC-numbers increased slightly from test D03 to D04a and b.

Fig. 13 shows the measured deformation of the scour protections over time for the tests from Deltares (2024) and Schendel et al. (2014) mentioned above. The deformation development is shown together with the development according to eq. 8 for time scale from 0.25 h to 8.0 hours, from which the time scale of each test has been estimated. A similar plot for the 10 applicable tests from Ferradosa (2018) is shown in Fig. 14. The time scales, corresponding non-dimensional time scales, and other basic data for each of the tests are listed in Tables 3 and 4. The non-dimensional time scale is defined as, see e.g. Sumer and Fredsøe (2002):

$$T^* = \frac{\left(g\left(s-1\right)D_{50}^3\right)^{1/2}}{D_p^2}T \tag{10}$$

It is note that the temporal resolution of most of the cases listed in Tables 3 and 4 is relatively low for these kinds of analyses and it is also noted that the scour protection may have settled slightly when submerged at the first time which may led to a slight overestimation of the deformation between initial condition and the deformation after the first test. If this is the case, the time scales based on the first test will tend to be underestimated. As for the deformation, see Sec. 3.2.6, there may be an effect of the D_{50}/D_p ratio, but it is not possible to identify it due to the limited amount of data. Furthermore, if there is an effect, it is likely not to affect the present results for the same reasons presented in Section 3.2.6.

The non-dimensional time scales, T^*, listed in Tables 3 and 4 are varying significantly by five orders of magnitude. The variation is mainly depending on the Shields and u_{cw}-number; however, by introducing the adjustment for the Shields number ($T^*/\theta^{-3/2}$) suggested by Larsen and Fuhrman (2023) the numbers become more aligned. The main variation is then due to the u_{cw}-number as for the live-bed conditions reported by Petersen et al. (2012) and Sumer et al. (2013) (as presented by Larsen and Fuhrman (2023)). However, as discussed in Sec. 3.1.1 regarding the MOB-number, the Shields number comes with a significant uncertainty that will be added to the uncertainty of the non-dimensional time scale, so the uncertainty of the time scale will be larger. This is found acceptable as the time scale depends on the mobility of the rock, usually represented by the Shields number, so it is not found possible not to have to add the uncertainty associated with the Shields number at some point during the process of predicting or estimating the time scale, as it is the case for predicting time scales of live-bed scour, see e.g. Larsen and Fuhrman (2023) and Sumer and Fredsøe (2002).

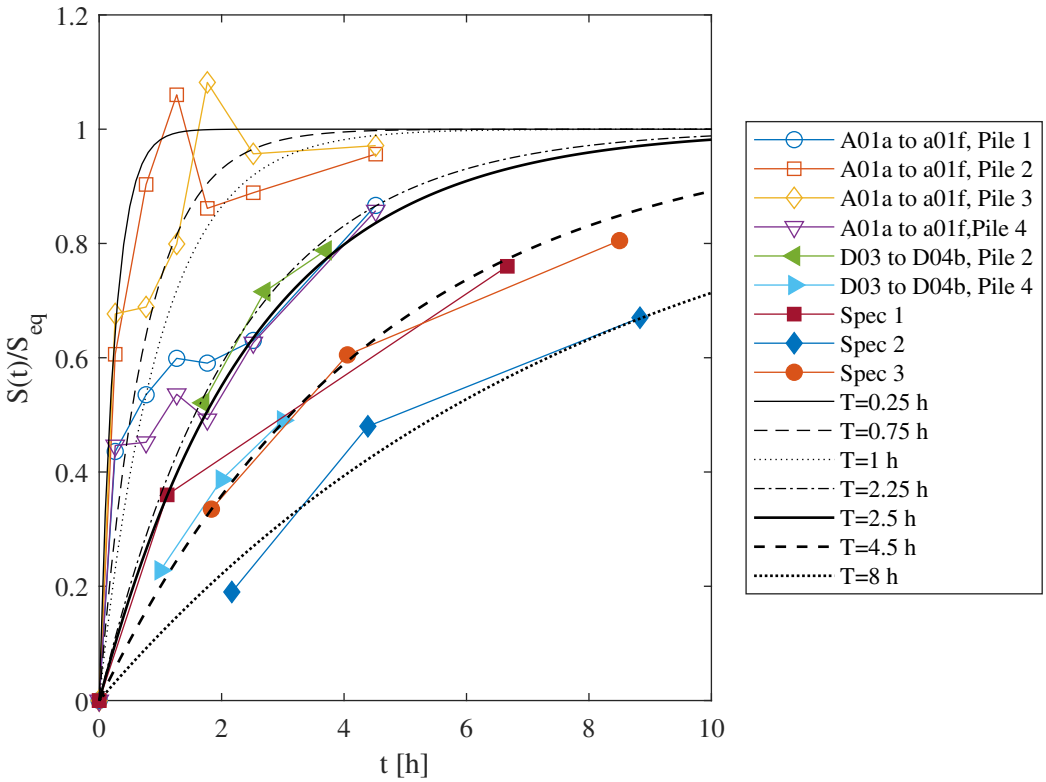

Figure 13: Deformation of scour protection as function of time. Time series A01a to A01f and D03 to D04b are from Deltares (2024), while Spec 1 to 3 are from Schendel et al. (2014). Fitting curves according to eq. 8 is included for relevant time scales.

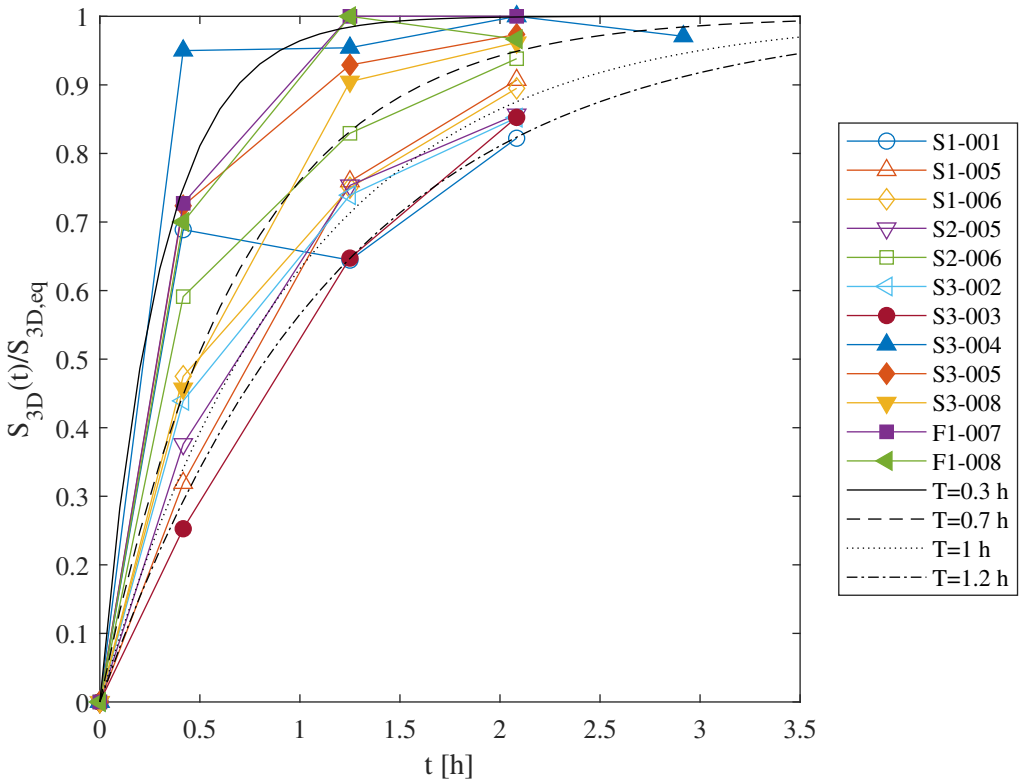

Figure 14: Deformation of scour protection as function of time. Time series are from Ferradosa (2018). Fitting curves according to eq. 8 is included for relevant time scales.

Table 3: Dimensional and non-dimensional time scales and various parameters for the time scale shown in Fig. 15 (excluding tests from Ferradosa (2018), see Table 4). Case 1 to 4 are test A01a to A01f Pile 1 to 4 and Case 5 to 6 are test D03 to D04b Pile 2 and 4, all from Atlantic Basin tests, Deltares (2024). Case 7 to 9 are from Schendel et al. (2014). Case 10 to 13 are test Uni01 to Uni03 and Tide 01 from Schendel et al. (2018). Case 14 and 15 are B1 and B2 from de Lemos et al. (2023). Note, the Shields number is calculated by the author, while the MOB_{top} is as provided in the respective datasets. The time scale, $T^*/\theta^{-3/2}$, estimated using Eq. 15 (Column 5) is based on the coefficients: $\Psi_c = 0.02$, $b_1 = 0.36$, and $b_2 = 5$. The KC-number was in the range 1.5 to 4.4 and the h/D_p was in the range 2 to 6.3.

Case	Est. T [h]	T^*	$T^*/\theta^{-3/2}$	$T^*/\theta^{-3/2}$, Eq. 15	Est S_{eq} [mm]	θ	u_{cw}	KC	MOB_{top}	D_p [cm]	s	D_{50} [mm]
1	2.5	69	0.38	0.31	95	0.030	0.42	1.5	0.78	30	3.15	2.8
2	0.25	32	0.16	0.30	60	0.028	0.43	2.2	0.62	20	2.70	5.0
3	0.75	94	0.44	0.30	55	0.028	0.43	2.2	0.65	20	2.70	4.9
4	2.5	1475	4.8	0.32	95	0.021	0.42	3.0	0.45	15	2.70	9.3
5	2.25	57	0.35	0.27	24	0.033	0.36	3.6	0.72	20	2.70	4.9
6	4.5	1026	6.4	0.27	75	0.033	0.36	3.6	0.73	15	2.70	5.0
7	4.5	86	0.15	0.020	25	0.014	0	2.4	-	100	2.65	12.0
8	4.5	86	0.32	0.020	100	0.024	0	3.4	-	100	2.65	12.0
9	8.0	152	1.0	0.020	200	0.036	0	4.4	-	100	2.65	12.0
10	1.9	3.1	0.0065	0.033	-	0.016	1	N/A	0.35	15	2.65	0.19
11	1.9	3.1	0.011	0.033	-	0.023	1	N/A	0.50	15	2.65	0.19
12	1.8	3.1	0.022	0.033	-	0.038	1	N/A	0.80	15	2.65	0.19
13	2.3	3.9	0.029	0.033	-	0.038	1	N/A	0.81	15	2.65	0.19
14	6.8	37	0.089	0.053	60	0.018	1	N/A	0.50	8	2.65	0.18
15	2.7	15	0.11	0.053	94	0.027	1	N/A	0.77	8	2.65	0.18

Table 4: Dimensional and non-dimensional time scales and various parameters for the time scale based on Ferradosa (2018) as shown in Fig. 15. The time scale, $T^*/\theta^{-3/2}$, estimated using Eq. 15 (Column 5) is based on the coefficients: $\Psi_c = 0.02$, $b_1 = 0.36$, and $b_2 = 5$. The pile diameter, D_p, was 10 cm for all tests, the KC-number was in the range og 2 to 3 and h/D_p in the range 2.4 to 5.0.

Test	Est. T [h]	T^*	$T^*/\theta^{-3/2}$	$T^*/\theta^{-3/2}$, Eq. 15	Est $S_{3d,eq}$	θ	u_{cw}	KC	s	D_{50} [mm]
S1-001	1.2	1.1	3.5	0.20	0.45	0.021	0.49	2.6	2.65	7.5
S1-005	1.0	0.20	1.3	0.16	14	0.034	0.53	2.5	2.56	2.7
S1-006	0.95	0.36	1.5	0.14	2.0	0.025	0.55	2.4	2.60	4.1
S2-005	1.0	0.20	1.4	0.21	8.8	0.037	0.49	2.7	2.56	2.7
S2-006	0.70	0.27	0.94	0.15	3.4	0.023	0.57	2.2	2.60	4.1
S3-002	1.0	0.38	2.2	0.17	2.3	0.033	0.55	2.1	2.60	4.1
S3-003	1.1	0.42	1.4	0.13	1.9	0.022	0.62	2.1	2.60	4.1
S3-004	0.40	0.15	0.49	0.13	2.4	0.022	0.62	2.1	2.60	4.1
S3-005	0.50	0.010	0.47	0.14	3.8	0.028	0.60	2.2	2.56	2.7
S3-008	0.30	0.12	0.54	0.14	1.05	0.022	0.61	2.2	2.60	4.1
F1-007	0.40	0.15	0.78	0.020	0.33	0.030	0	2.8	2.59	4.1
F1-008	0.45	0.17	1.0	0.020	0.30	0.033	0	3.0	2.59	4.1

3.4.1 Prediction of time scales

Larsen and Fuhrman (2023) provided a formula for estimating the time scale of scour around a monopile in combined waves and current under live-bed conditions:

$$\frac{T^*}{\theta^{-3/2}} = \begin{cases} \Psi(KC)\left[\left(\frac{0.18}{\Psi(KC)}\right)^{\frac{1}{0.44}}\right]^{u_{cw}} & \text{for } u_{cw} < 0.44,\ KC \geq 4,\ \frac{h}{D_p} < 27 \\ \Omega(h/D_p)u_{cw}^{\ln(\frac{0.18}{\Omega(h/D_p)})/\ln(0.44)} & \text{for } u_{cw} \geq 0.44,\ KC \geq 4,\ \frac{h}{D_p} < 27. \end{cases} \tag{11}$$

where:

$$\Psi\left(KC\right) = 8 \cdot 10^{-5} KC^{2.5} \tag{12}$$

and (h being the water depth):

$$\Omega\left(\frac{h}{D_p}\right) = \frac{1}{375}\left(\frac{h}{D_p}\right)^{0.75} \tag{13}$$

Equation 11 for live-bed conditions has the same trend as the time scales for clear water scour and scour protection deformation, see Fig. 15. For both clear water and live-bed conditions the time scale is relatively low for waves alone and steady current, but somewhat higher for combined waves and current. It should, however, be noted that the amount of clear water data is limited, so it cannot be confirmed that the peak of the time scale in clear water and live-bed conditions appears at the same u_{cw}-number. Looking at the available data it seems like the non-dimensional time scale for clear water is around 100 to 1000 times longer than for live bed in case of waves alone, around 1 to 100 times longer at u_{cw} around 0.4, and approximately 1 to 20 times longer in steady current.

The relatively longer time scale for waves compared to steady current should be seen in relation to differences between equilibrium scour depth in clear water contra live-bed conditions for waves and steady current. In the case of steady current, the maximum relative equilibrium scour depth is approximately the same for clear water and live-bed conditions, see e.g. de Lemos et al. (2023). In case of waves the maximum equilibrium scour depth in clear water conditions are up to around three times larger than the live-bed equilibrium scour for the present range of KC-numbers, see e.g. Fig. 10. The larger relative equilibrium scour depth for clear water scour compared to live-bed conditions will take longer to scour and the time scale will consequently have to increase more for waves compared to steady current.

It must, furthermore, be noted that the estimated time scales are associated with considerable uncertainty. This is especially the case for the time scales estimated on the basis of data of relatively poor temporal resolution, which is the case for all data presented in the entire Sec. 3.4 except the de Lemos et al. (2023) data. For this reason, and due to the low numbers of datapoints, it is strongly advised to apply these data with great care. The necessity of verifying works based on these data by reliable methods, e.g. physical model tests and suitable numerical simulations should

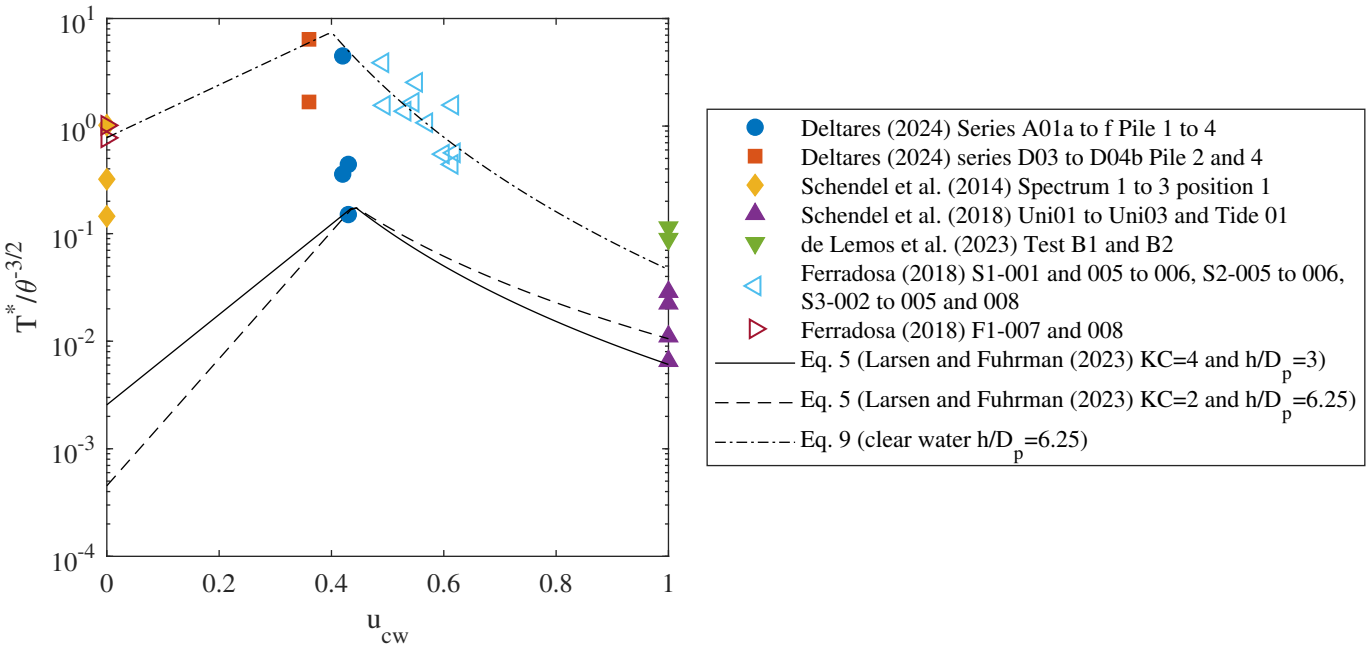

Figure 15: Non-dimensional time scales of scour protection deformation and clear water scour from different studies plotted together with predicted time scales for live-bed conditions according to Larsen and Fuhrman (2023). Data for each point can be found in Tables 3 and 4. The data for Ferradosa (2018) is based on S_{3D} rather than S/D_p.

also be considered. This can include evaluating the safety level of the design, consequences of failure, type of failure among other issues.

3.4.2 Adaptation of equation 11 for clear water conditions

The value of a formula for estimating the time scale is high, especially if it can be combined with the formula for equilibrium deformation, Eq. 7. If both the time scale and the equilibrium deformation can be predicted, it can be used in a time step model to predict the development of the deformation over time and thereby work around the issue that it is difficult to assess the actual deformations from actual storms as the deformation depends both on intensity and duration of the storm, see also Sec. 3.2. Therefore Eq. 11 is adapted to clear water conditions, despite the relatively high uncertainty of the available data and the limited number of data points.

As for the formula by Larsen and Fuhrman (2023) the formula for clear water deformation will give $T^*/\theta^{-3/2}$ as function of u_{cw}. The formula will also consist of two parts: one for wave dominated and one for current dominated conditions. In the case of wave dominated conditions the time scale presented by Larsen and Fuhrman (2023) depends on the KC-number. However, as discussed in Sec. 3.2.1, the KC-number had little impact on the deformation for the small KC-number in the present study; this is also found to be the case for the time scale where there is no clear trend between $T^*/\theta^{-3/2}$ and the KC-number in the dataset or the wave dominated (u_{cw} separated, see Tables 3 and 4. Analyses have shown that both the correlation and $MALE$ (Mean Absolute Logarithmic Error, Eq. 14) improves when the dependency on the KC-number is omitted.

$$MALE = \frac{1}{N_{obs}} \sum_{i=1}^{N_{obs}} \left| \ln \left(\frac{P_i}{O_i} \right) \right| \tag{14}$$

where N_{obs} is the number of observations, P is the predicted value, and O is the observed value.

The best correlation and $MALE$ for the data in Table 3 and 4 was found to be for the coefficients $\Psi_c = 0.78$, $b_1 = 7.47$, and $b_2 = 4.4$ in Eq. 15 and 16. It was also found that both correlation and MALE improved slightly by reducing the change from wave to current condition from $u_{cw} = 0.44$ in Larsen and Fuhrman (2023) to $u_{cw} = 0.4$. This gives a correlation of 0.6 and $MALE = 0.8$.

Fig. 15 includes an example of a result of Eq. 15 with the coefficients given in the previous paragraph. The formula is generally following the data points fairly well with an exception of three data points from Deltares (2024) test series A, which appears to have a relative time scale, $T^*/\theta^{-3/2}$, around ten to fifty times smaller than the rest of the data.

It has not been possible to identify a reason for the large spreading of the dimensionless time scale, $T^*/\theta^{-3/2}$, for u_{cw} around 0.4, but seen in Figs. 13 and 14 the time scale based on the tests series A in Deltares (2024) is the best temporarily resolved time series for determining the time scale (except for the time scales by de Lemos et al. (2023) time scales for steady current with very high temporal resolution). Inspecting Fig. 13 shows that the development of the deformation in case of Deltares (2024) test series A is uneven with many changes and even reduced deformation over time in some cases, similar to the variations often seen in scour tests, see e.g. Silva-Muñoz and Broekema (2025). Silva-Muñoz and Broekema (2025) in fact suggest a more detailed definition of the time scale that takes variations like this into account. However, while Deltares (2024) test series A may have sufficient data to conduct an analysis as described in Silva-Muñoz and Broekema (2025), the remaining data set will not provide sufficiently high resolution time series for this kind of analysis and it is therefore decided to apply the traditional definition of the time scale in Eq. 8.

Nevertheless, the above coefficients found in the analysis provide a poor result of the time step model (see Sec. 3.5). The time scale based on these coefficients is too long and leads to a significant underestimation of the scour protection deformations in the time series provided by Deltares (2024) and Schendel et al. (2014). To account for this, the coefficients were modified to provide a better result when applied in the time step model, but on the expense of the capability to reproduce the estimated time scales in Table 3 and 4. The modified formula reads:

$$\frac{T^*}{\theta^{-3/2}} = \begin{cases} \Psi_c \left[\left(\frac{b_1}{\Psi_c} \right)^{\frac{1}{0.4}} \right]^{u_{cw}} & \text{for } u_{cw} < 0.4,\ KC < 5.5,\ \frac{h}{D_p} < 6 \\ \Omega_c(h/D_p) u_{cw}^{\ln(\frac{b_1}{\Omega_c(h/D_p)})/\ln(0.4)} & \text{for } u_{cw} \geq 0.4,\ KC < 5.5,\ \frac{h}{D_p} < 6. \end{cases} \tag{15}$$

where:

$$\Omega_c \left(\frac{h}{D_p} \right) = \frac{b_2}{375} \left(\frac{h}{D_p} \right)^{0.75} \tag{16}$$

and $\Psi_c = 0.02$, $b_1 = 0.36$, and $b_2 = 5$. Valid for rough bed on the scour protection (in practice constant critical Shields number) and Shields numbers smaller than approximately 0.035.

An example of the time scale calculated by Eq. 15 is shown as a thick black line in Fig. 15. It is clear that it is not following the data as closely as previously given parameters, but it is still within the scatter of the data for current dominated conditions where it follows the time scales of Deltares (2024) Test Series A better; time scales that are considered of higher quality. It should also be recalled that the time scale based on data from Ferradosa (2018) is based on S_{3D} instead of S/D_p and this may have impacted the magnitude of the time scale. For wave conditions, the proposed formula gives a time scale 10 to 100 times smaller than the data in Table 3. The time scales for waves in the table is based on a few time steps and is consequently uncertain, which is found to be the main reason for the difference.

For the formula to provide the best possible estimate of the time scale it is important to use the correct input parameters, see Sec. 4.3.1 for details. The procedure for calculating the parameters is outlined in App. C.

3.5 Time step model for deformation of scour protections around monopiles

When formulas are established to determine equilibrium deformation (Eq. 7) and the time scale of the process (Eq. 15) with a reasonable accuracy these can be used to estimate the development over time. The methodology is the same as applied in time step models for scour development, see e.g. Nielsen and Hansen (2007); Raaijmakers and Rudolph (2008); Harris et al. (2010) and most recently Silva-Muñoz and Broekema (2025) for time step models for scour around monopiles.

The basic concept is that deformation goes towards a certain equilibrium deformation and time scale given by the hydrodynamic conditions, monopile, and scour protection material. This is described by the equation:

$$S_n = S_{eq,n} + (S_{n-1} - S_{eq,n}) \exp\left(-\frac{dt}{T_n} \right) \tag{17}$$

where S_n and $S_{eq,n}$ are the deformation and equilibrium deformation after the n^{th} time step, respectively, S_{n-1} is the deformation in the previous time step, dt is the time step, and T_n is the time scale of the deformation for the n^{th} time step.

The time step model has been applied to the test series provided by Deltares (2024) for Atlantic Basin tests, as shown in Fig. 16. The accuracy of the model varies from test series to test series as could be expected from the accuracy of

the prediction of the equilibrium deformation and time scale of the deformation, Eqs. 7 and 15, respectively. However, overall the model follows the trend of the deformation observed in the model tests. The model is also applied for the results from Delta Flume provided in Deltares (2024) and the results from Großer Wellenkanal (GWK) by Schendel et al. (2014) as shown in Fig. 17. It is clear that there is a significant difference between the time scale of the Deltares (2024) Delta Flume results and the Schendel et al. (2014) GWK results. This is despite that the tests are conducted in almost similar wave conditions and scale. The main differences were the peak wave periods, which were 4.0 to 5.3 s in the Delta Flume and 8.0s s in GWK, however, not enough to explain the large difference (the KC-numbers were 1 to 2 and 2 to 4 for the Delta Flume and GWK, respectively. The median rock sizes were also similar: 9 mm and 18 mm for Delta Flume and 12 mm for GWK. However, the gradation varied a lot; the GWK tests had $D_{16}/D_{84} = 7.4$ and the Delta Flume was $D_{15}/D_{85} = 3.5$ and 25.3. Again, not a good explanation as the GWK gradation was in between the two Delta Flume results.

A final difference was identified as the placement of the rock. In Delta Flume the rock was placed as a traditional scour protection with an overall extent of $3D_p$, while it in the GWL tests was place as an elevated bed over the entire width of the flume and 4.5 m up- and downstream of the pile centre. This may explain the result as the larger extent reduces the risk of loosing rocks over the edge of the scour protection, a process that will speed up the deformation process.

The performance of the model on the time series shown in Figs. 16 and 17 is shown in Fig. 18. The correlation (0.7) and an $RMSE = 0.05$ which are both reasonable. The model provides reasonable accurate results with a weak tendency to overpredict the deformation in case of large deformation, S/D_p larger than around 0.15.

3.5.1 Limitations to the time step model

The time step model is fully based on empirical data which does not cover the entire span of the model and also come with some uncertainty. The lack of data and general uncertainty of the data will impact the accuracy of the model and also limit the conditions of which it can be applied. The overall limitations of the model are:

- Little data on equilibrium deformation for the most wave dominated conditions ($u_{cw} < 0.35$).
- Little data on equilibrium deformation for current dominated conditions ($u_{cw} > 0.75$)
- Little equilibrium deformation data for Shields numbers above 0.028 and no data above 0.036
- Generally little data on the time scale
- Generally high uncertainty on the time scale data
- No data on time scale for most wave dominated conditions ($0 < u_{cw} < 0.35$).
- No data on time scale for most wave dominated conditions ($0.65 < u_{cw} < 1.0$).

Of these limitations the most important are assessed to be the limit on the Shields number and the general uncertainty of the time scale. Given the available data it is not possible to improve the time scale coverage, so until additional time scale data become available this uncertainty has to be accepted, if the model is applied.

For the equilibrium deformation it must be kept in mind that the deformation may be underestimated in general and this may influence the entire result of the model. The actual impact on the result depends on the actual metocean conditions as well as how big the error in the assumed wave induced deformation actually is, which is unknown. In general it is strongly recommended not to apply the model for Shields numbers larger than 0.025, as larger Shields numbers tends to give significantly increased uncertainty of the output. Furthermore, the model cannot be considered valid outside the range of $0.5 < KC < 5.5$ and should only be applied for hydraulic rough scour protections (constant critical Shields number).

In addition to the requirement of $\theta < 0.025$ it must be kept in mind that the model is only valid for scour protections around monopiles with an extent of minimum 3 times the pile diameter, $w_{sp}/D_p \geq 3$. It is also important to emphasise that the model is only valid for deformation of the armour layer. Any deformation into layers under the armour layer (filter layer and natural seabed materials) is not included in the model and the deformation is likely to be underestimated if this happens. Likewise, effects of seabed level changes (general seabed level changes and moving bed forms) as well as edge scour is not included.

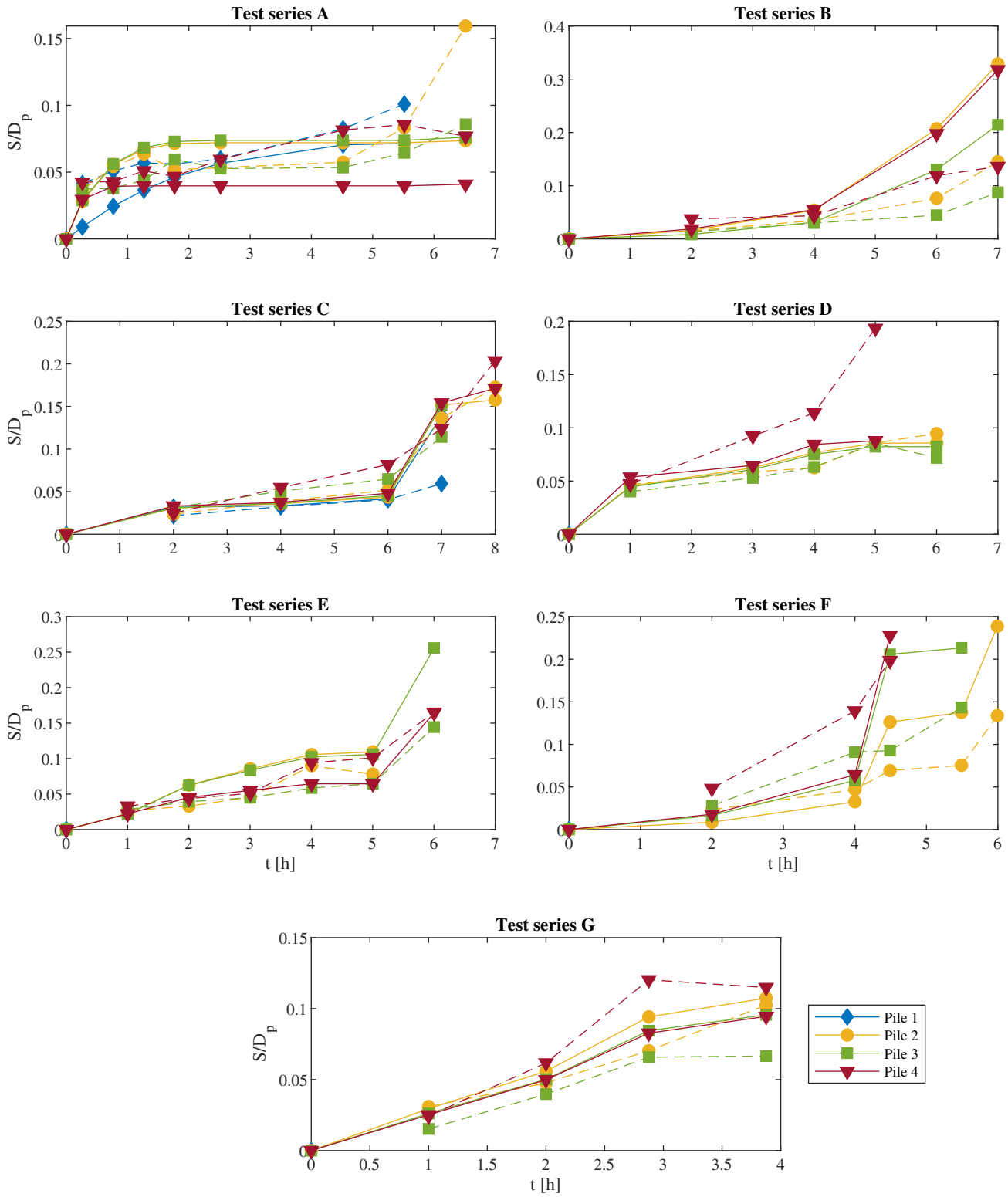

Figure 16: The time step model applied on the time series from the Atlantic Basin tests provided by Deltares (2024). The observed development is shown with dashed lines, and the predicted deformation is shown with fully drawn lines. Tests with a scour protection extent less than $3D_p$ are omitted. Tests with breakthrough of the armour layer ($S > t_{sp} - D_{50}$) are likewise omitted.

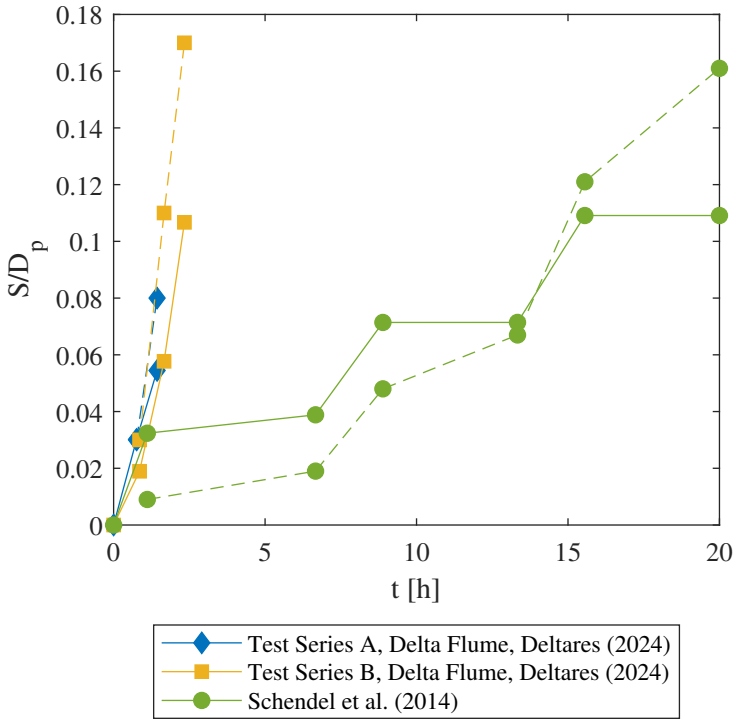

Figure 17: The time step model applied on the time series provided by Deltares (2024) for the Delta Flume tests and the tests by Schendel et al. (2014). The observed development is shown with dashed lines, and the predicted deformation is shown with fully drawn lines. Tests with breakthrough of the armour layer ($S > t_{sp} - D_{50}$) are omitted.

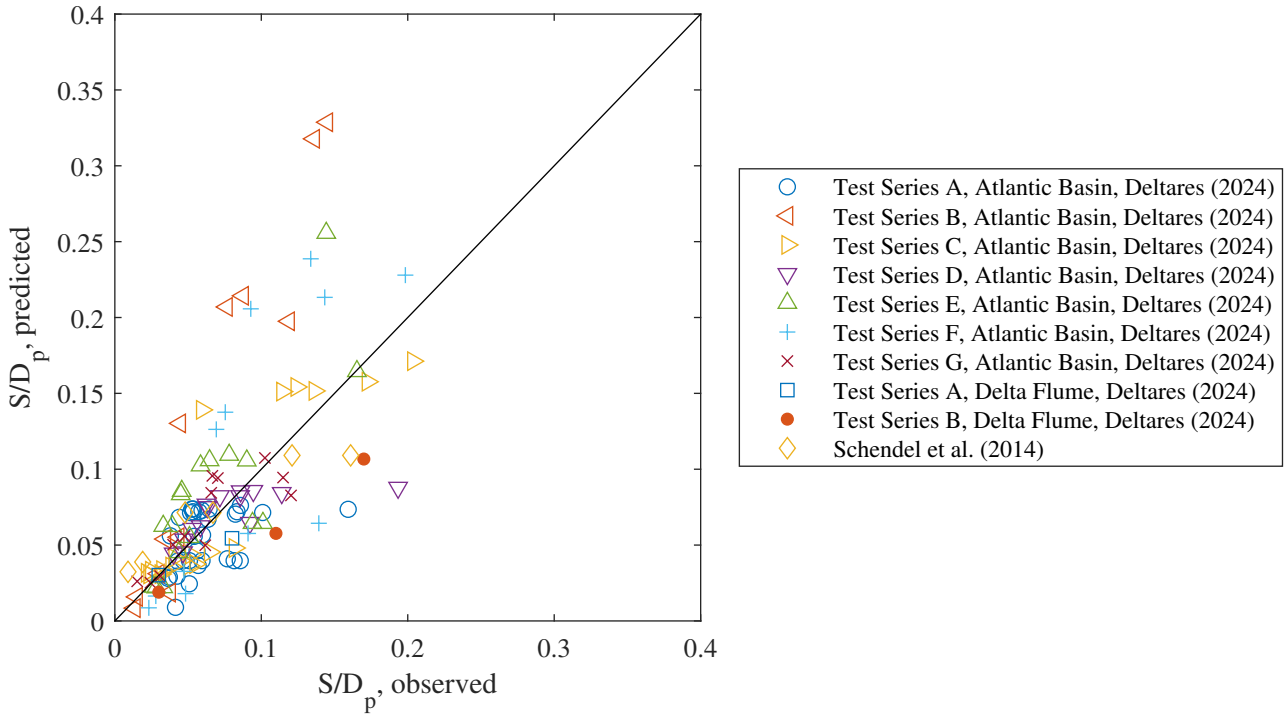

Figure 18: The performance of the time step model on the time series presented in Figs. 16 and 17. The correlation between the observed deformation and the predicted is 0.7 while RMSE=0.04.

4 Comparison of different design criteria

Over the past decades different design criteria have been proposed. Common design methods are the criteria proposed by den Boon et al. (2004) and de Vos et al. (2012). Where the criteria by den Boon et al. (2004) is recommended in DNV (2022). Also, the criteria proposed by Broekema et al. (2024) must be mentioned among well-known methods. Finally, Nielsen and Petersen (2019) presented criteria primarily based on data from de Vos et al. (2012). These criteria are similar to the present model for equilibrium deformation, as it is based on u_{cw} and the Shields number, but instead of providing the relative equilibrium deformation, S_{eq}/D_p, it provided a qualitative description of the damage: "Low damage", "Some motion", and "Failure", based on the criteria defined by de Vos et al. (2012).

It is relevant to compare the equilibrium deformation formula (Eq. 7) and the time step model with these deformation and design criteria. It is noted that not all the above-mentioned criteria can be compared directly as they do not provide directly comparable outputs. The present model and Broekema et al. (2024) can be compared as both provide the relative deformation, S/D_p. The formula by de Vos et al. (2012) provides the dimensional number S_{3D}, which is essential also S/D_p but averaged over an area equal to the cross-sectional area of the monopile. There is of course a relation between the maximum deformation S/D_p, as applied in this study, and S_{3D}, but the relation is uncertain, so it is not found feasible to derive and apply this relation. However, the criteria will be compared qualitatively and based on an a rough relation between S_{3D} and the qualitative description of the deformation also adapted by Nielsen and Petersen (2019).

Furthermore, only Nielsen and Petersen (2019) and the present model provides the results directly as function of the Shields number and u_{cw}, while the other criteria depend indirectly on these parameters. It is therefore not feasible to make a general comparison between the criteria, but to compare different examples by varying u_m and V so $0 \leq u_{cw} \leq 1$ is covered while other input parameters are kept constant. The selected examples and the parameters are listed in Table 5 and the results for the different criteria are shown in Fig. 19.

4.1 Design method proposed by den Boon et al. (2004)

Den Boon et al. (2004) proposed a simple design method based on the relative Shields number $MOB = \theta/\theta_{cr}$ and has three limits:

1. Limited movement: $MOB < 0.415$
2. Some movement: $MOB < 0.460$
3. Significant movement: $MOB \geq 0.460$

As seen in Fig. 19 the method appears reasonable for wave dominated conditions, u_{cw} smaller than around 0.4 to 0.5. Although it should be mentioned that it allows a larger deformation for waves alone compared to combined waves and current. For higher u_{cw} numbers the criteria have some significant limitations. If applied for current dominated conditions (u_{cw} larger than around 0.5) it will result in significant deformations of the scour protection up to around a pile diameter. Such large deformation will in most practical applications be regarded a failure of the scour protection. Scour protections in current dominated conditions will be discussed further in section 3.2.7.

As the criteria is based on MOB it is necessary to determine the critical Shields number to compare it to the present results and to apply it for practical applications. As discussed in Sections 3.1.1 and 3.2.2 this comes with a significant uncertainty. As shown in Section 3.2.2 the critical Shields number varies from 0.03 to 0.06 at the constant and, for this purpose, most relevant part of the Shields curve, and as previously shown, this interval may even be larger when waves and combined waves and current are considered. However, just considering the interval of the critical Shields number of 0.03 to 0.06 may result in both "Limited movement" and "Significant movement", just depending on the selection of critical Shields number. A similar variation appears for u_{cw} numbers from 0 up to around 0.5, where the variation is larger than the difference between the two limits.

It seems reasonable to apply the criteria for conditions with u_{cw} smaller than around 0.4 to 0.5. In this case a deformation around $S_{eq}/D_p = 0.05$ can be expected; however, it is not likely that there will be a practical effect of differentiating between "Limited movement" and "Some movement" given the small difference and general scatter of the deformation.

Table 5: The input parameters applied for the selected examples to compare the equilibrium deformation formula (Eq. 7) with the criteria by den Boon et al. (2004), de Vos et al. (2012), and Broekema et al. (2024). The relative density of the rock and the density of the water is kept constant at $s = 2.65$ and $\rho_w = 1000$ kg/m^3, respectively.

Criteria	Case	θ_{cr}	u_m [m/s]	V [m/s]	T_p [s]	h [m]	D_p [m]	D_{50} [m]	N	S_{3D}	S/D_p
den Boon et al. (2004)	-	0.055	N/A	N/A	N/A	N/A	N/A	N/A	N/A	N/A	N/A
de Vos et al. (2012)	1	N/A	0.82 to 0	0 to 1.56	14.0	20.0	8.0	0.15	3000	1	N/A
de Vos et al. (2012)	2	N/A	1.30 to 0	0 to 2.41	14.0	20.0	8.0	0.30	3000	1	N/A
de Vos et al. (2012)	3	N/A	0.72 to 0	0 to 1.56	17.0	20.0	8.0	0.15	3000	1	N/A
Broekema et al. (2024)	4	0.055	1.40 to 0	0 to 3.79	12.0	20.0	8.0	0.15	N/A	N/A	0.05
Broekema et al. (2024)	5	0.045	0.166 to 0	0 to 0.476	1.6	0.364	0.145	0.0027	N/A	N/A	0.05
Broekema et al. (2024)	6	0.055	1.71 to 0	0 to 4.41	12.0	20.0	8.0	0.30	N/A	N/A	0.05
Broekema et al. (2024)	7	0.055	1.71 to 0	0 to 4.41	15.0	20.0	8.0	0.15	N/A	N/A	0.05
Broekema et al. (2024)	8	0.055	1.46 to 0	0 to 3.53	12.0	20.0	8.0	0.15	N/A	N/A	0.025

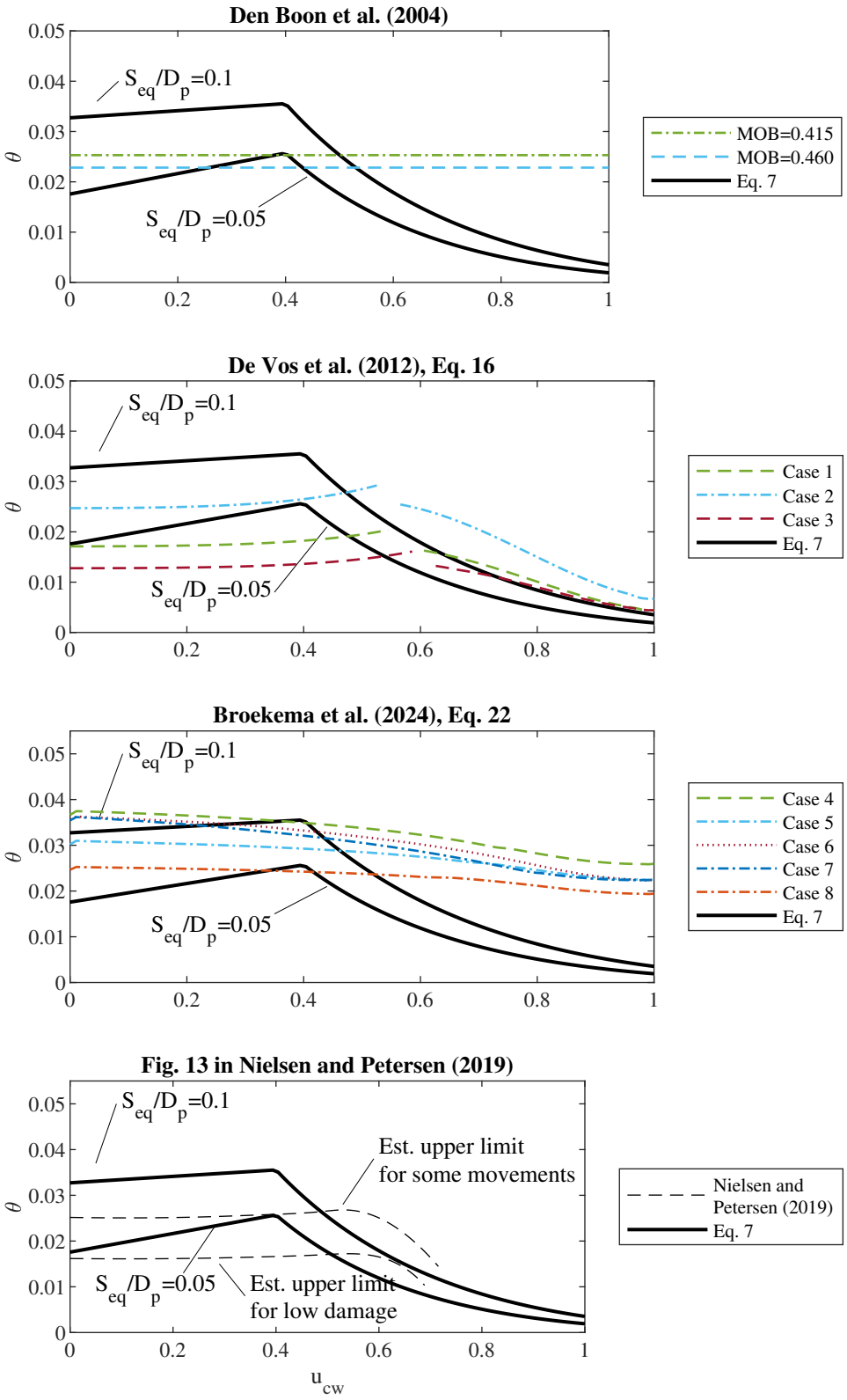

Figure 19: Results of different methods for predicting armour rock sizes for monopiles compared to the method given by Eq. 7. The comparison is based on the cases listed in Table 5. It should be noted that the Shields and u_{cw} numbers for results of Broekema et al. (2024) has been adjusted to account for the different definition of u_m in the study by Broekema et al. (2024) and this study, see Sec. 4.3.1 for details.

4.2 Design method proposed by de Vos et al. (2012)

The criteria by de Vos et al. (2012) is an empirical formula based on relatively small scale physical model tests. The formula reads:

$$\frac{S_{3D}}{N^{b_0}} = a_0 \frac{u_m^3 T_{m-1,0}}{\sqrt{gh}(s-1)^{3/2} D_{n50}^2} + a_1 \left(a_2 + a_3 \frac{\left(\frac{V}{w_s}\right)^2 (V + a_4 u_m)^2 \sqrt{h}}{g D_{n50}^{3/2}} \right) \tag{18}$$

where S_{3D} is a non-dimensional damage number, N is the number of waves, $T_{m-1,0}$ is the energy spectral wave period, $D_{n,50}$ is the nominal median size of the rock, and w_s is the fall velocity of the armour rock. b_0, a_0, a_1, a_2, a_3, and a_4 are fitting coefficients. According to de Vos et al. (2012) the different coefficients and parameters can be set or calculated as follows: $b_0 = 0.243$, $a_0 = 0.00076$, $a_2 = -0.022$, and $a_3 = 0.0079$. The coefficient a_1 is defined as:

$$\begin{aligned} a_1 &= 0 \text{ for } \frac{V}{\sqrt{g D_{n50}}} < 0.92 \text{ and waves following current} \\ a_1 &= 1 \text{ for } \frac{V}{\sqrt{g D_{n50}}} \geq 0.92 \text{ or waves opposing current} \end{aligned} \tag{19}$$

In the examples in this article waves following current is applied.

The parameter a_4 is:

$$\begin{aligned} a_4 &= 1 \text{ for waves following current} \\ a_4 &= \frac{Ur}{6.4} \text{ for waves opposing current} \end{aligned} \tag{20}$$

where $Ur = L^2 H_{m0} h^3$ is the Ursell number and L is the wave length calculated for a regular wave with period $T = T_{m-1,0}$. Again, in the examples in this article waves following current is applied.

The energy spectral wave period is assumed to be $T_p = 1.107 T_{m-1,0}$ (as for a standard JONSWAP spectrum). The fall velocity of the armour rock is set to:

$$w_s = 1.1[(s-1) g D_{50}]^{0.5} \text{ for } D_{50} \geq 1 \text{ mm} \tag{21}$$

Three cases of the result of Eq. 18 are shown in Fig. 19. It is noted that Fig. 19 present the damage as function of u_{cw} and the Shields number but that these numbers are not direct input parameters to Eq. 18. To be able to plot the result of the equation this way all input parameters and the result (damage number) have been kept constant for each case, except the velocities, u_m and V which has been varied to cover $0 \leq u_{cw} \leq 1$. The input parameters for each case is listed in Table 5. Considering Case 1 it is seen that the formula tends to follow the overall trend of Eq. 7. The obtained relation between the Shields number and u_{cw}-ratio is reasonable for the entire range of u_{cw}, although it is to the low side for the intermediate range $0.3 < u_{cw} < 0.6$. Considering that S_{3D} was set to 1 corresponding to damage level 3: "significant movement of stones, without failure of the protection" (de Vos et al., 2012), the obtained Shields numbers is also reasonable with a relative deformation of the scour protection, S_{eq}/D_p, a around 0.05. For this description a Shields number around 0.04 would be expected for wave dominated conditions.

It is also noted that Eq. 18 takes the duration of a condition into account in terms of number of waves. However, the predicted damage number S_{3D}, does not go towards an equilibrium but continues to increase for increasing number of waves. This is misleading as the deformation will go towards an equilibrium if the exposure is long enough in the clear water regime for the armour rock. The time scale is discussed further in Sec. 3.4.

Furthermore, Eq. 18 appears to be sensitive to variations in both the rock size (Case 2) and the wave period (Case 3), which make results of the formula unreliable and questionable for practical applications when Froude scaling is most often applied.

It is noted that the discontinuity of the curves representing Eq. 18 is due to a discontinuity in the formula when the parameter a_1 change between 0 and 1.

4.3 Discussion of the design formula for deformation of scour protections by Broekema et al. (2024)

Based on the Deltares (2024) data and data not publicly available, Broekema et al. (2024) presented a design formula for prediction of deformation of the scour protection around a monopile (50% confidence):

$$\frac{S}{D_p} = f\left(KC_{tot}\right) \cdot 0.07 MOB_{top}^{1.65} \tag{22}$$

Where S is the deformation of the scour protection, MOB_{top} is the ratio of the undisturbed Shields number to the critical Shields number measured at the top of the scour protection and $f(KC_{tot})$ is a function of a modified Keulegan-Carpenter number, KC_{tot}, defined as:

$$KC_{tot} = \frac{\left(u_m + V\right) T_p}{D_p} \tag{23}$$

Where u_m is the amplitude of the horizontal wave induced orbital velocity at the top of the scour protection as defined in eq 8 in Broekema et al. (2024), V is the depth averaged current velocity, T_p is the peak period, and D_p is the diameter of the monopile. The function $f(KC_{tot})$ is defined as:

$$f\left(KC_{tot}\right) = 1 + \frac{3.93}{1 + \exp\left(-0.74 KC_{tot} + 4.75\right)} \tag{24}$$

The function, $f(KC_{tot})$, is, according to Broekema et al. (2024), introduced to account for the increasing amplification of the flow around the pile for increasing KC-numbers, as reported by Sumer et al. (1997). However, it must be noted that Sumer et al. (1997) applied the traditional definition of the KC-number ($KC = u_m T/D_p$) and did not report amplifications in the case of combined waves and current. The results from Sumer et al. (1997) and Broekema et al. (2024) can therefore not be compared directly, but it is correct that Sumer et al. (1997) reported increasing amplification for increasing KC-number which is in line with the fact that the flow become more and more current-like with increasing KC-numbers. As an argument for applying $f(KC_{tot})$ Broekema et al. (2024) furthermore states: "Wave related bed shear stress amplification as a function of the KC-number is shown by Sumer et al. (1997) to steadily increase from a value of $KC_w \approx 2.8$ until it stabilizes at a value of $KC_w \approx 10$. Given that in the present study the combined effect of the waves and current are considered, the values described here match remarkably well with the findings from Sumer et al. (1997)." However, it is unclear which data in Sumer et al. (1997) this refers to as Fig. 18 in Sumer et al. (1997) indicates that the amplification continues to increase for KC-numbers up to at least 100. Also Fig. 14 in Sumer et al. (1997) shows that the separation distance will continue to increase until at least $KC = 20$. It is also noted that the stabilisation of $f(KC_{tot})$ for KC_{tot} larger than around 9 takes place outside the range of KC_{tot} (and also KC as this is, by definition, the same or smaller than KC_{tot}) covered by the dataset as the dataset covers KC_{tot} from little more than 0 to just below 8 with a single data point at around $KC_{tot} = 10.5$, see Fig. 6 in Broekema et al. (2024). The definition of the $f(KC_{tot})$ does also have the implications that the predicted deformation will not increase for KC_{tot} larger than approximately 15 and constant MOB_{top}. The maximum predicted deformation will be $S/D_p = 0.35$ ($MOB_{top} = 1$ and $KC_{tot} > 15$), but this is much smaller than have been reported for clear water current and waves, where $S/D_p = 1.18$ (de Lemos et al., 2023) and 0.5 (Nielsen et al., 2023) were reported for current and waves, respectively.

By replacing the traditional representation of the flow by the KC and u_{cw} with the KC_{tot}, Broekema et al. (2024) loses important information. KC_{tot} is firstly unphysical as the product of VT_p has no physical meaning, as there is no direct relation between current speed and wave period. Secondly, as wave induced velocity and current speed is only represented by a sum and not a ratio (e.g. u_{cw}), the KC_{tot} does not differentiate between wave and current dominated conditions, which have been demonstrated in Sec. 3.1 and 3.2.6, and by Nielsen and Petersen (2019) to be important for scour protection deformation.

An example can illustrate this. Consider test conditions with co-directional waves and current where the sum of wave induce velocity and current velocity is constant ($u_m + V = 1.5$ m/s), the same monopile ($D_p = 8.0$ m) and Shields number large enough to cause deformation but not live-bed, set to $\theta = 0.03$, of the scour protection, and a peak period, $T_p = 12$ s. D_{50} is varied to account for the variations of the bed shear stress over the range of u_{cw}. The result of this is shown in Fig. 20 where the upper panel shows the deformation as function of u_{cw} while the lower panel shows the required median rock size to obtain a constant Shields number of 0.03 again as function of u_{cw}. Eq. 22 (Broekema et al., 2024) provide a constant deformation for all values of u_{cw}, while the present formula provides an almost constant deformation for the wave dominated conditions ($u_{cw} < 0.4$) but slightly increasing for increasing u_{cw}. The increase in deformation in the current dominated conditions can also be expected; Nielsen and Petersen (2019) showed that the horseshoe vortex will initiate motion for Shields numbers larger than around 0.006 to 0.018 in steady current. De Lemos et al. (2023) reported scour of $S/D_p = 1.18$ for a similar Shields and MOB-number, and similar results were reported by Qu et al. (2024), based on several previous studies.

The lower panel of Fig. 20 show the required median rock size to obtain the target Shields number ($\theta = 0.03$) as function of u_{cw}. The overall trend is that the required rock size decreases with increasing u_{cw}. The required rock

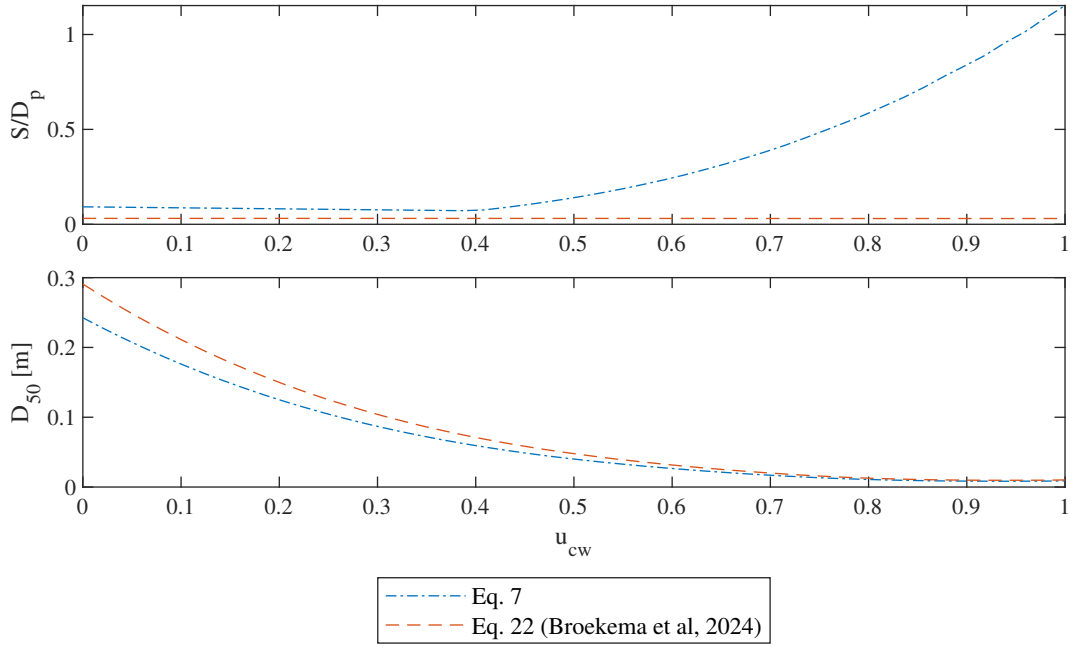

Figure 20: Relative deformation (upper panel) and required median rock size (lower panel) to keep a constant Shields number of 0.03 for different combination of waves and current when the summarised velocity ($u_m + V = 1.5$ m/s). Pile diameter, $D_p = 8.0$ m, peak wave period, $T_p = 12$ s, water depth, $h = 20$ m, density of water, $\rho_w = 1000$ kg/m^3, and the relative densitty of the rock, $s = 2.65$, were kept constant.

size in waves alone is found to be 0.24 m and 0.29 m for Eq. 22 (Broekema et al. (2024)) and Eq. 7, respectively. The required rock sizes reduce to 10 mm and 9 mm for steady current. This reflect the fact that the bed shear stress for a given summarised velocity ($u_m + V$) and roughness is smaller for current dominated conditions than for wave dominated conditions provided typical wave periods. Nevertheless, given the small median rock size for current dominated conditions and the high amplification of the of the bed shear stresses under these conditions (see e.g. Hjorth (1974) compared to waves (see e.g. Sumer et al. (1997)) it is clear that a significant deformation will develop.

This is further supported by the previously mentioned test reported by de Lemos et al. (2023) (Test B2). The water depth, current velocity, and sediment size of the test were approximately Froude scale 1:40 of the example above (the pile diameter was smaller), and had a relative scour depth of $S/D_p = 1.18$ or 39 times larger than the relative deformation predicted using Eq. 22 by Broekema et al. (2024). Furthermore, it should be recalled that for the present data ($0.5 < KC < 5.5$) the influence of the KC-number on the scour protection deformation has been found to be small, see Sec. 3.1 and 3.2.1.

Broekema et al. (2024) did notice that there could be an effect of the wave-current ratio not covered by the methodology outlined in Eq. 22 to 24. In Table 2 and Fig. 12 in Broekema et al. (2024) three cases with similar MOB_{top} and KC_{tot} but varying wave-current ratios were given. These tests were identified as seen in table 6 listed as Case 1 to 3, where the key parameters as well as deformation type is listed. The table does also include other tests with lower Shields numbers and while the deformation type for the three tests considered by Broekema et al. (2024) are all categorised as Type 2, all three deformation types are represented when the Shields number is reduced from around 0.03 to around 0.02 with practically constant KC_{tot}. This is a strong indication that KC_{tot} is not a good representation for the flow conditions. It should be noted that not all of the tests in Table 6 are at equilibrium according to the criteria given in Sec. 3.2.1; this is the case for Test ID: G04-Pile 4, B03-Pile 3 both Deltares (2024), and 08B (Wu et al., 2020).

The formula has been tested for variations in rock size and wave period and the impact on the result is small. In addition, the result of the Base Case in linear scale 1:55 has been added to illustrate the effect of Shields versus MOB-scaling, see Sec. 3.1.1. If Shields scaling was applied there would be no difference between Base Case and the scaled Base case, but as seen in Fig. 19 the scaled results have lower Shields numbers for the same deformation, i.e. it is conservative.

Finally, it is seen in Fig. 19 that it tends to overestimate the stability of the rock. The Base Case is set to have a relative deformation of 0.05 but it has Shields number around the 0.1 relative deformation curve in case of wave dominated conditions. In case of current the difference increases and the formula by Broekema et al. (2024) fails to

Table 6: Examples of deformation types with Shields numbers around 0.03 (examples from Table 2 in Broekema et al. (2024)) and tests with Shields numbers around 0.02, both cases with varying wave-current ratios. "case" in column two of the table refers to the Case number in Broekema et al. (2024) Table 2.

Test ID	Case	MOB_{top}	θ	KC_{tot}	KC	u_{cw}	Est. S_{eq}/D_p	Deform. Type
G04, Pile 4	3	0.68	0.031	5.1	5.1	0.00	-	2
A03, Pile 2	1	0.69	0.031	6.4	4.0	0.38	0.16	2
B04, Pile 2	2	0.65	0.027	5.6	1.6	0.70	0.15	2
A01f, Pile 4	-	0.43	0.020	5.1	2.9	0.43	0.08	1
B03. Pile 3	-	0.43	0.018	5.1	1.7	0.64	-	2
08B (Wu et al., 2020)	-	0.38	0.020	5.4	1.2	0.78	-	3
B1 (de Lemos et al., 2023)	-	0.50	0.018	-	-	1.00	0.75	3

predict the trend as the effect of the horseshoe vortex is not included in the formula. Given this, the formula can be considered unreliable for $u_{cw} > 0.4$. For smaller u_{cw}-ratios, it is closer to a reliable, but not significantly better than e.g. den Boon et al. (2004), which is much simpler. Nevertheless, it is important to apply the right definition of u_m as this can have a major impact on the results.

As for de Vos et al. (2012), Eq. 22 does not depend directly on u_{cw} and the Shields number, so as in Sec. 4.2 the curves have been calculated by applying most input parameters and the resulting deformation as constants while varying u_m and V to cover $0 \leq u_{cw} \leq 1$. The input parameters for each case is listed in Table 5.

4.3.1 Reproducebility and sensitivity of the model by Broekema et al. (2024) and the present study

The Broekema et al. (2024) formula (Eq. 22), the present formula for equilibrium deformation (Eq. 7), and the time step model (Eq. 17) all provide relative deformation, S/D_p. For this reason, these formulas can be compared more or less directly for a given relevant dataset.

Broekema et al. (2024) reported a correlation of 0.85 and an $RMSE = 0.016D_p$ for the formula in Eq. 22 and the dataset applied by Broekema et al. (2024). However, only parts of that dataset is publicly available, as described in Sec. 4.3, so a more detailed comparison of the results of the two methods is shown in Fig. 21, based on the Atlantic Basin test series in Deltares (2024) dataset. It is seen in the left panel that the time step model has less good correlation, 0.69, compared to Eq. 22 with a correlation of 0.77 (right panel), however, it should be noted that the Atlantic Basin test series in Deltares (2024) dataset only covers a narrow range of u_{cw}, primarily in the wave dominated part.

For a more general dataset the Broekema et al. (2024) method is performing significantly worse than the time step model can be expected to do. Fig. 22 shows the performance of Eq. 22 on the dataset applied for Figs. 11 and 12 and it is clear that the equation underpredict the deformation by de Lemos et al. (2023) significantly by a factor around 3.5, while Eq. 7 provided a reasonable prediction, see Fig. 12, and this is also the case for the time scale (Eq. 15) so the time step model will give reasonable results in the case. This also shows that Broekema et al. (2024) method should be applied with great care as it may underpredict the deformation significantly, without any clear indications as no limitations for the formula is provided.

It must also be noted that the predicted relative deformation, S/D_p, depends strongly on u_m. Predicted by the Broekema et al. (2024) method it will for example be underestimated by around a factor of 1.7 if u_m is calculated in the way apply in this article compared to the way it is defined in Broekema et al. (2024). This is due to a difference of around 10% to 20% in the predicted u_m which results in a difference of the Shields number around 10% which consequently also apply for MOB_{top}. This shows that both methods are rather sensitive to even smaller variations in the definitions of hydrodynamic forcing and it is strongly adviced to follow the definition applied for the development of the method used, see also App. C for the present methodology. Furthermore, it is noted that the definition of u_m applied by Broekema et al. (2024) is applied when results of Eq. 22 is presented in this article to show the correct performance of the equation.

4.4 Design method proposed by Nielsen and Petersen (2019)

Going back to Fig. 19, the lowermost panel compare the present results with the criteria by Nielsen and Petersen (2019). Nielsen and Petersen (2019) presented the stability of the armour in the similar way as the present study,

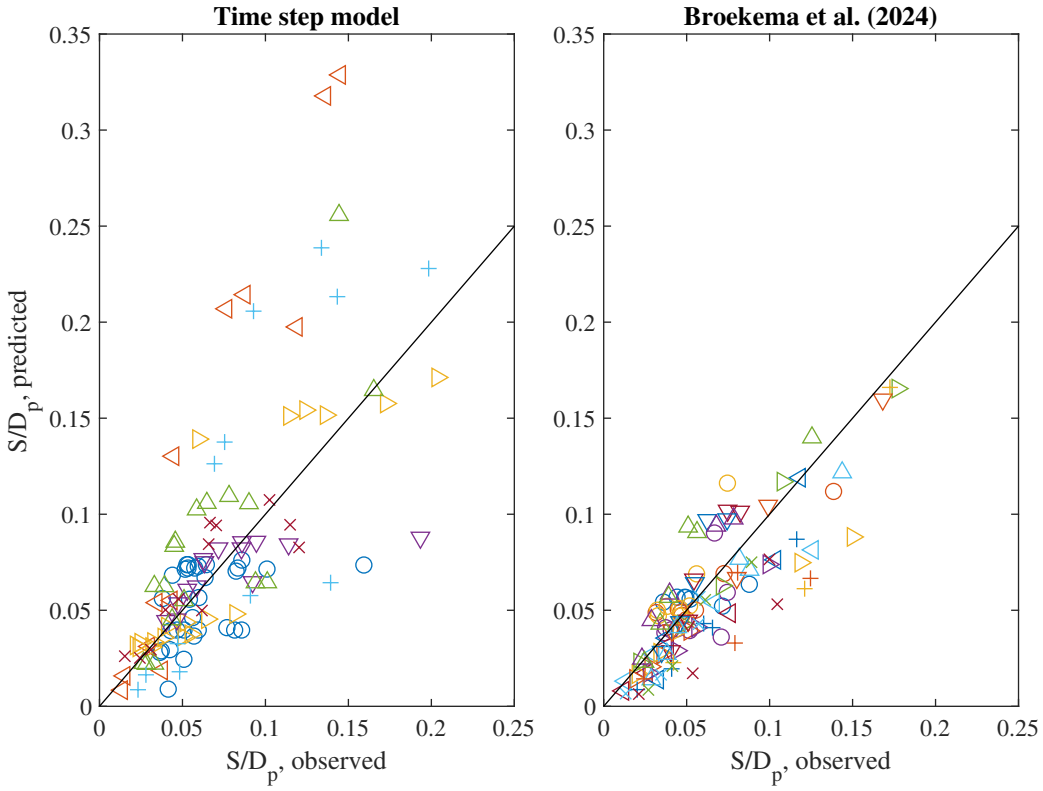

Figure 21: The performance of the time step model (Eq. 17) and the model by Broekema et al. (2024) (Eq. 22) for different input parameters. The upper right panel shows the performance of the time step model with present S/D_p and u_m. The upper left panel shows the same, but for Eq. 22. The lower panels show likewise the time step model and the Eq. 22 but with u_m directly from Deltares (2024) and the observed S/D_p reduced by a factor of 1.15. Symbols as in Fig. 18.

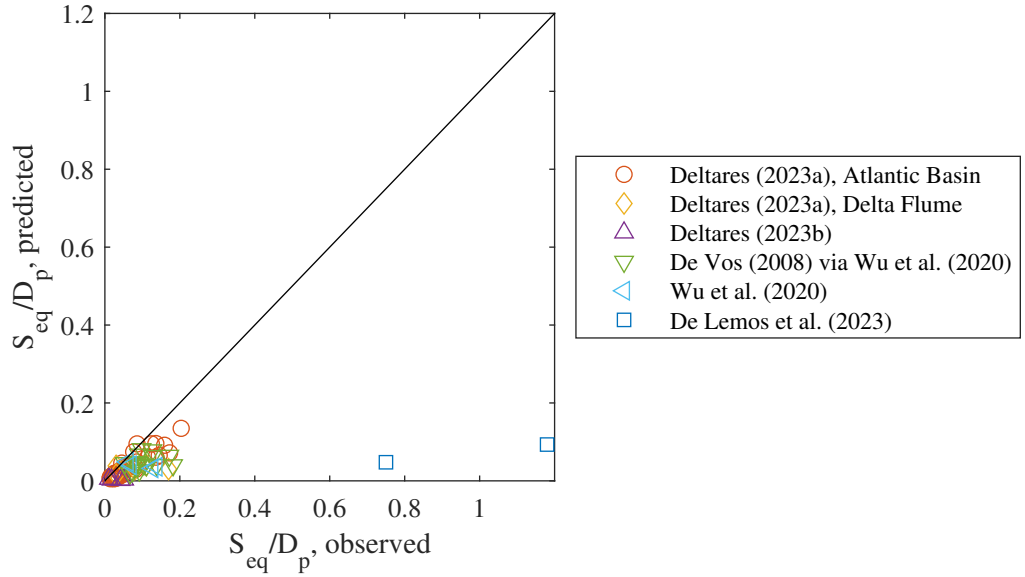

Figure 22: The performance the model by Broekema et al. (2024) (Eq. 22) on the dataset of equilibrium deformations applied in the present study and as presented in Fig. 11. $KC_{tot} = 20$ was applied for steady current cases, giving maximum $f(KC)$, Eq. 24.

as function of the u_{cw}-ratio and the Shields number, which was divided into three groups: "low damage", "some movements", and "failure" based on data from de Vos et al. (2012), which again is based on the definition of damage proposed by den Boon et al. (2004). The two limits between the three categorizes of deformation is given in the panel together with the present results.

There is a good agreement for combined waves and current (u_{cw} around 0.4) where the estimated upper limit of "some movements" follows the $S_{eq}/D_p = 0.05$ curve which seems reasonable, also if compared to Fig. 5 where this limit is at the estimated limit between Type 1 and 2 damage. However, as for den Boon et al. (2004); de Vos et al. (2012); Broekema et al. (2024) the criteria by Nielsen and Petersen (2019) do not get the reduced stability in the most wave dominated conditions and it is likely that the deformation will be the same for "estimated upper limit for low damage" in waves alone as it is for "estimated upper limit for some movements" in the case of combined waves and current.

For more current dominated conditions, $u_{cw} > 0.4$ the present study and Nielsen and Petersen (2019) is not aligned. The criteria by Nielsen and Petersen (2019) for these conditions have higher Shields values than expected from the present study. It is noted that the present study is based on a larger dataset in the relevant range of u_{cw} ($0.4 < u_{cw} < 0.7$).

It is, furthermore, noted that the results in Nielsen and Petersen (2019) were based on $u_s = \sqrt{2}u_m$. The curves have been adjusted to follow the definition of the orbital wave induced velocity applied in this article (u_m).

5 Remarks regarding practical applications of the results

This article presents three main results that can be of practical use in the design of scour protections. The three results are:

- Estimated equilibrium deformation depth
- Estimated time scales of the deformation process
- A time step model for predicting the development of the deformation

However, these results cannot be applied directly without due consideration of the conditions of which they are applied as well as the associated uncertainties of the results. As mentioned previously, the equilibrium deformation can in many cases be a conservative estimate of the actual deformation; especially if it is designed for a relative infrequent event and the time scale of that event is long. In some cases, a time scale of several days for full scale conditions are reasonable to assume. This should be compared to a typical duration of the design storm around 3 to 6 hours in which case the actual deformation caused by a single storm can be as little as 5% to 10% of the equilibrium deformation, assuming the deformation according to Eq. 8.

The potential conservatism by applying equilibrium deformation can be reduced by applying the time step model, see Sec. 3.5. However, while the equilibrium deformation comes with some uncertainty, this can built-up in the time step model resulting in an increased uncertainty of the results. This is especially the case if only one or a few time series are applied in the time step model. It is recommended to apply a large number of realistic time series to get an estimate of the uncertainty of the model. It is also important to ensure that the limitations of the model are respected ($\theta < 0.025$ and $0.5 < KC < 5.5$) and consider if the model is seriously affected by the limitations described in Sec. 3.5.1. With a large number of realisation, it is possible to assess the expected deformation of the scour protection over the life time, considering the required safety and in this way optimise the rock size in the scour protection. If this outlined method is applied, especially if the resulting deformation is large, it is recommended to identify the events causing the large deformations and have these tested by physical model tests or suitable numerical simulations. In the decision on whether such events shall be tested, the u_{cw}-ratio and Shields numbers of the event can also be considered; are they in a well-documented space (see Fig. 11) or are the predicted deformation based on significant interpolation in which case additional verification in terms of physical model tests or suitable numerical simulations is strongly recommended, especially if the design accept high Shields numbers or are current dominated.

5.1 Other effects on the deformation of scour protections

The present re-analysis of data in the literature focuses on the three classic non-dimensional parameters: Shields and KC-numbers and the wave-to-current ratio u_{cw}. The application of these parameters, in particular Shields number and

u_{cw}-ratio, has shown good results. However, it is also clear that these three parameters do not cover all relevant aspects of the deformation of scour protections and other effects may be important, at least in some situations. Examples of effects that are not considered in the re-analysis but is likely to influence the deformation in some cases are 1) gradation of the rock material, 2) shape of the rock, 3) edge scour, scouring and possible armouring of the surrounding seabed, and 4) marine growth on the scour protection.

In the re-analysis the rock size is represented by the median rock size, D_{50}. However, if the gradation of the rock becomes wide enough there may be an armouring effect of the scour protection where the finest fractions of the scour protection is washed away while the coarser materials remain in place, as described by Petersen et al. (2018) for current. If an armouring process take place to a significant degree, the D_{50} of the initial rock gradation will no longer be representative for the stability of the remaining rock and if a sufficiently large amount of the coarser material remain in place it will reduce the deformation of the scour protection. However, most of the model tests are conducted with narrow or fairly narrow graded rock so this effect has not been considered in the present study.

The shape of rock will also have an impact om the stability. However, the vast majority of the model tests are conducted with angular crushed rock and this and blasted rock is also the most common material for prototype scour protections. This effect has not been considered, first of all because very limited data are available for other than crushed rock and secondly because the practical relevance of other shapes is limited.

The interaction between the scour protection and the surrounding seabed is an important factor in the scour protection design, especially for scour protections with small extent (typically $w_{sp}/D_p < 3$)., as it may have had for the time scale in case of Schendel et al. (2014), see Sec. 3.5. If the horizontal extent of the scour protection becomes small enough, dynamic rocks in the amplified flow around the pile on top of the scour protection will reach the edge and roll down the scour protection. This can eventually reduce the thickness of the scour protection to a critical level. This effect is largely governed by edge scour (see e.g. Petersen et al. (2015)), and seabed lowering due to moving bed forms and general seabed lowering, all process that can be reduced by armouring of the seabed in a similar way as armouring of the scour protection as described in the paragraph above. However, this is a specialised effect that is not covered systematically by the available model tests.

Finally, marine growth could have an effect. Usually, marine growth is not considered for scour protection design, as also stated in DNV (2022). That said, marine growth may have both positive and negative effects on the stability of the scour protection. In general, marine growth will have a lower density than the rock and combined with an increased surface area, it will reduce the stability of the rock. On the other hand, some types of marine growth may connect the individual rock in a way that increases the overall stability, although this is usually not considered for design as the development of this marine growth takes time and is uncertain. Furthermore, no relevant data is found so it has not been considered.

6 Conclusions

Studies of armour rock stability around monopiles from the past two decades have been reviewed and re-analysed. The review has shown that the available studies cover many relevant aspects of the stability of armour rock around monopiles, including descriptions of the mechanisms causing deformation of the scour protections, qualitative description of the deformations of the scour protections under different conditions and well as quantitative descriptions of the deformations. Furthermore, the review did also show that the approach of the physical model testing and postprocessing of the results applied in the different studies has varied. This has caused some issues in comparing the results of different studies and should be kept in mind when working with these data to avoid misleading interpretations.

The re-analysis of the data has shown that the data is well inline with the methodology outlined by Nielsen and Petersen (2019). The results of the different studies all appear to be a function of the Shields number and the u_{cw}-number, while the KC-number has a smaller impact on the results; this is attributed to the low KC-numbers applied in the applied studies ($0.5 < KC < 5.5$). Both the qualitative (pattern of deformation) and quantitative (S_{eq}/D_p) deformation are presented as function of Shields number and the u_{cw}-number, with a good correlation between the two representations.

The time scale of the scour protection deformation has been determined and presented together with time scales of clear water scour. It was found that the non-dimensional time scales for clear water scour and scour protection deformation followed the same trend as live-bed scour with relatively short time scale for waves alone and steady current and slightly longer time scales for combined waves and current. However, the time scales appeared, depending primarily on the u_{cw}-number, to be around 1 to 1000 longer than what was predicted by Larsen and Fuhrman (2023) formula for live-bed scour. The largest increase in time scale is found to be for waves alone.

Parametrisations of both the equilibrium deformation depth and the time scale have been proposed. The parametrisations have been applied in a time step model to predict the development of the deformation over time. The model provided results in reasonable agreement with results of physical model tests after an adjustment of the parametrisation of the time scale, which reduced the difference between clear water and live-bed conditions significantly.

The review and re-analysis have unveiled some lack of data that would improve the prediction of the deformation, especially the prediction by the time step model if available. Most of the available data for equilibrium deformation data are concentrated in the range $0.3 < u_{cw} < 0.7$, which make predictions outside this range extra uncertain. There is also a general lack of data for Shields numbers above 0.035 and below 0.01; however, the latter is less important as the deformations can be expected to be very small.

The time scales are generally very uncertain as they are for the most part based on very little data. At the same time, the time step model is rather sensitive to the time scale. For this reason, it is found to be a major benefit for the time step model if better time step data was available. This applies for the entire range of u_{cw}-ratio and the relevant range of Shields numbers.

Acknowledgements

Acknowledgements to Dr. Minghao Wu for his support in understanding the data behind the Wu et al. (2020) study as well as his, Dr. Leen de Vos', and Prof. Peter Troch's effort of providing the reanalysed data from de Vos (2008) and Dr. Yorick Broekema for his support in the understanding of the JIP HaSPro dataset (Deltares, 2024). I acknowledge Dr. Niels Gjøl Jacobsen and Mr. Palle Martin Jensen for fruitful discussions on this subject and Prof. B. Mutlu Sumer, Dr. Thor Ugelvig Petersen, Dr. Niels Gjøl Jacobsen, and Dr. Yorick Broekema for the many relevant comments that have helped improving this article significantly. I thank the reviewers for their effort and thorough reviews.

Author contributions (CRediT)

Not applicable for single-author paper.

Funding

This study was financially supported by DHI A/S through a grant from a research contract with the Danish Ministry of Higher Education and Science (contract 1034-00001B) and by NIRAS through a grant (Grant Agreement No. 101136087) from the European Commission to the budget of the Inf4inity project (https://inf4inity.com/). The support is gratefully acknowledge.

Use of AI

No AI was used in the preparation of this work.

Data access statement

Source and processed data are available at Zenodo: https://doi.org/10.5281/zenodo.17387774. The material includes a datafile for each of the data sources and a readme file describing the data in the datafiles and provide the references to the original sources.

Conflict of interest (COI)

There is no conflict of interest.

Notations

Name	Symbol	Unit
Coefficients for parametrisation of equilibrium deformation	a_1, a_2, a_3	-
Area for calculation of S_{3D}	A	m^2
Coefficients for parametrisation of time scale	b_1, b_2	-
Median rock size	D_{50}	m
Nominal median rock size	$D_{n,50}$	m
Pile diameter	D_p	m
Acceleration due to gravity	g	m/s^2
Keulegan-Carpenter number	KC	-
Total Keulegan-Carpenter number (including steady current)	KC_{tot}	-
Hydraulic roughness of scour protection	k_s	m
Wave length	L	m
Mean Absolute Logarithmic Error	$MALE$	-
Mobility number (θ/θ_{cr})	MOB	-
Mobility number (θ/θ_{cr}) at the initial top of scour protection	MOB_{top}	-
Number of waves	N	-
Number of observations	N_{obs}	-
Observed value	O	"Depends"
Predicted value	P	"Depends"
Reynolds number	Re	-
Relative density of rock	s	-
Maximum deformation of scour protection	S	m
Maximum equilibrium deformation of scour protection	S_{eq}	m
Damage number	S_{3D}	-
Equilibrium damage number	$S_{3D,eq}$	-
Thickness of scour protection	t_{sp}	m
Time	t	s and h
Time scale of the deformation process	T	s and h
Non-dimensional time scale of the deformation process	T^*	-
Energy spectral wave period	$T_{m-1,0}$	s
Peak wave period	T_p	s
Ratio between wave and current velocities	u_{cw}	-
Wave induced orbital velocity amplitude at the initial top of scour protection	u_m	m/s
Friction velocity	U_f	m/s
Depth averaged current velocity	V	m/s
Volume of deformation	V_s	m^3
Fall velocity	w_s	m/s
Overall extent of top of scour protection	w_{sp}	m
Kinematic viscosity	ν	m^2/s
Maximum wave and current induced bed shear stress	τ_{max}	N/m^2
Shields number	θ	-
Critical Shields number	θ_{cr}	-
Density of water	ρ_w	kg/m^3
Grain density of rock	ρ_r	kg/m^3
Estimated error of the number	Δ	-

References

Arboleda Chavez, C.E., Stratigaki, V., Wu, M., Troch, P., Schendel, A., Welzel, M., Villanueva, R., Schlurmann, T., de Vos, L., Kisacik, D. et al. (2019). Large-scale experiments to improve monopile scour protection design adapted to climate change—the proteus project. *Energies*, **12**(9), 1709.

Baker, R.E. (1986). *Local scour at bridge piers in non-uniform sediment*, Master's thesis, University of Auckland, at Auckland, New Zealand.

Broekema, Y., van Steijn, P., Wu, M. and Robijns, T. (2024). Predicting loose rock scour protection deformation

around monopiles using the relative mobility number and the keulegan–carpenter number. *Ocean Engineering*, **300**, 117475.

Chambel, J., Fazeres-Ferradosa, T., Bento, A., Taveira-Pinto, F. and Lomónaco, P. (2023). Experimental study of long-term scour damage for protected offshore wind foundations, In: *Advances in the Analysis and Design of Marine Structures*, 235–244, CRC Press.

Corvaro, S., Marini, F., Mancinelli, A., Lorenzoni, C. and Brocchini, M. (2018). Hydro-and morpho-dynamics induced by a vertical slender pile under regular and random waves. *Journal of Waterway, Port, Coastal, and Ocean Engineering*, **144**(6), 04018018.

de Lemos, S., Leandro, A.B., Nielsen, A.W. and Roulund, A. (2023). Experimental study of clear water and low kc number wave-current scour around xl monopiles, In: *11th International Conference on Scour and Erosion*, International Society for Soil Mechanics and Geotechnical Engineering.

de Schoesitter, P., Audenaert, S., Baelus, L., Bolle, A., Brown, A., Das Neves, L., Ferradosa, T., Haerens, P., Pinto, F.T., Troch, P. et al. (2014). Feasibility of a dynamically stable rock armour layer scour protection for offshore wind farms, In: *International Conference on Offshore Mechanics and Arctic Engineering*, volume 45411, V003T10A026, American Society of Mechanical Engineers.

de Sonneville, B., Joustra, R. and Verheij, H. (2014). Winnowing at circular piers under currents, In: *Scour and Erosion: Proceedings of the 7th International Conference on Scour and Erosion, Perth, Australia, 2-4 December 2014*, 203, CRC Press.

de Sonneville, B., van Velzen, G., Verheij, H. and Dorst, K. (2012). Falling aprons at circular piers under currents, In: *ICSE 6: Proceedings of the 6th International Conference on Scour and Erosion, Paris, France, 27-31 August 2012*, Société Hydrotechnqiue de France (SHF).

de Vos, L. (2008). *Optimisation of scour protection design for monopiles and quantification of wave run-up - Engineering the influence of an offshore wind turbine on local conditions*, Ph.D. thesis, Dept. of Civil Engineering, University of Ghent.

de Vos, L., de Rouck, J., Troch, P. and Frigaard, P. (2011). Empirical design of scour protections around monopile foundations: Part 1: Static approach. *Coastal Engineering*, **58**(6), 540 – 553. ISSN 0378-3839. DOI:10.1016/j.coastaleng.2011.02.001.

de Vos, L., de Rouck, J., Troch, P. and Frigaard, P. (2012). Empirical design of scour protections around monopile foundations. part 2: Dynamic approach. *Coastal Engineering*, **60**(0), 286 – 298. ISSN 0378-3839. DOI:10.1016/j.coastaleng.2011.11.001.

Deltares (2023*a*). *JIP HaSPro - WP2 External stability loose rock scour protection - Test specifications and factual test results*, Deltares.

Deltares (2023*b*). *JIP HaSPro - WP2 Flexibility of loose rock scour protection - Test specification and factual test results*, Deltares.

Deltares (2024). Jip haspro public data delivery (1.0) [data set], Zenodo. https://zenodo.org/records/10812205.

den Boon, J., Sutherland, J., Whitehouse, R., Soulsby, R., Stam, C., Verhoeven, K., Høgedal, M. and Hald, T. (2004). Scour behaviour and scour protection for monopile foundations of offshore wind turbines, In: *Proceedings of the European Wind Energy Conference*, volume 14, 26, EWEC London UK.

Dixen, F.H., Sumer, B.M. and Fredsøe, J. (2008). Suction removal of sediment from between armour blocks. part 2. waves. *Journal of Hydraulic Engineering, ASCE*, **134**(10), 1405–1420. ISSN 07339429, 19437900.

DNV (2022). *DNV-RP-0618 Rock scour protection for monopiles*, DNV.

Ferradosa, T.J.F.M. (2018). *Reliability Analysis Applied to the Optimization of Dynamic Scour Protections for Offshore Windfarm Foundations*, Ph.D. thesis, Universidade do Porto (Portugal).

Hansen, E.A., Simonsen, H.J., Nielsen, A.W., Pedersen, J. and Høgedal, M. (2007). Scour protection around offshore wind turbine foundations, full-scale measurements, In: *Scientific Proceedings of the European Wind Energy Conference 2007 (EWEC 2007)*, 132–138, http://www.ewec2007proceedings.info/index.php.

Harris, J.M., Whitehouse, R.J.S. and Benson, T. (2010). The time evolution of scour around offshore structures. *Proceedings of the Institution of Civil Engineers: Maritime Engineering*, **163**(1), 3–17. ISSN 17417597, 17517737. DOI:10.1680/maen.2010.163.1.3.

Hjorth, P. (1974). *Lokal erosion kring bropelare och rörledningar*, Institutionen för vattenbyggnad - Tekniska Högskolan i Lund, bulletin Serie A nr 30.

Larsen, B.E. and Fuhrman, D.R. (2023). Re-parameterization of equilibrium scour depths and time scales for monopiles. *Coastal Engineering*, **185**, 104356.

Loosveldt, N. and Vannieuwenhuyse, K. (2012). *Experimental validation of empirical design of a scour protection around monopiles under combined wave and current loading*, Master's thesis, Universiteit Gent, Belgium.

Mayall, R.O., McAdam, R.A., Whitehouse, R.J., Burd, H.J., Byrne, B.W., Heald, S.G., Sheil, B.B. and Slater, P.L. (2020). Flume tank testing of offshore wind turbine dynamics with foundation scour and scour protection. *Journal of Waterway, Port, Coastal, and Ocean Engineering*, **146**(5), 04020033.

Melville, B. and Sutherland, A. (1988). Design method for local scour at bridge piers. *Journal of Hydraulic Engineering*, **114**(10), 1210–1226.

Nielsen, A.W. and Hansen, E.A. (2007). Time-varying wave and current-induced scour around offshore wind turbines. *Proceedings of the International Conference on Offshore Mechanics and Arctic Engineering - OMAE*, **5**, 399–408.

Nielsen, A.W., Liu, X., Sumer, B.M. and Fredsøe, J. (2013). Flow and bed shear stresses in scour protections around a pile in a current. *Coastal Engineering*, **72**, 20–38.

Nielsen, A.W., Madsen, A.U., Christiansen, B.R. and Carstensen, S. (2023). Degradation of armour layer in a scour protection around a monopile exposed to waves, In: *11th International Conference on Scour and Erosion*, International Society for Soil Mechanics and Geotechnical Engineering.

Nielsen, A.W. and Petersen, T.U. (2018). Onset of motion of sediment underneath scour protection around a monopile. *Journal of Marine Science and Engineering*, **6**(3), 100.

Nielsen, A.W. and Petersen, T.U. (2019). Stability of cover stones around a vertical cylinder under the influence of waves and current. *Coastal Engineering*, **154**, 103563.

Nielsen, A.W., Probst, T., Petersen, T.U. and Sumer, B.M. (2015). Sinking of armour layer around a vertical cylinder exposed to waves and current. *Coastal Engineering*, **100**, 58–66.

Nielsen, A.W., Sumer, B.M., Fredsøe, J. and Christensen, E.D. (2010). Scour protection around offshore wind turbines. monopiles, In: *Proceedings of the Fifth International Conference on Scour and Erosion 2010*, volume 1, 440–449.

Nielsen, A.W., Sumer, B.M., Fredsøe, J. and Christensen, E.D. (2011). Sinking of armour layer around a cylinder exposed to a current. *Proceedings of the Institution of Civil Engineers - Maritime Engineering*, **164**(Ma4), 159–172.

Nielsen, A.W., Sumer, B.M. and Petersen, T.U. (2014). Sinking of scour protections at horns rev 1 offshore wind farm, In: *Proceedings of the International Conference on Coastal Engineering (ICCE 2014)*, 34.

Petersen, T., Nielsen, A., Hansen, D., Pedersen, A., Christensen, E. and Fredsøe, J. (2018). Stability of single-graded scour protection around a monopile in current, In: *Scour and Erosion IX*, 45–45, CRC Press.

Petersen, T.U., Sumer, B.M., Fredsøe, J., Raaijmakers, T.C. and Schouten, J.J. (2015). Edge scour at scour protections around piles in the marine environment—laboratory and field investigation. *Coastal Engineering*, **106**, 42–72.

Petersen, T.U., Sumer, B.M., Meyer, K.E., Fredsøe, J. and Christensen, E.D. (2012). Edge scour in current adjacent to stone covers, In: *Proc., 6th Int. Conf. on Scour and Erosion (ISCE-6)*, Société Hydrotechnique de France Paris.

Qu, L., An, H., Draper, S., Watson, P., Zhao, M., Harris, J., Whitehouse, R. and Zhang, D. (2024). A review of scour impacting monopiles for offshore wind. *Ocean Engineering*, **301**, 117385.

Raaijmakers, T. and Rudolph, D. (2008). Time-dependent scour development under combined current and waves conditions - laboratory experiments with online monitoring technique, In: *Proceedings Fourth International Conference on Scour and Erosion*, volume I, 152–161.

Raaijmakers, T., Van Oeveren, M., Rudolph, D., Leenders, V. and Sinjou, W. (2010). Field performance of scour protection around offshore monopiles, In: *Scour and Erosion*, 428–439.

Raaijmakers, T.C., Rudolph, D., Bergen, M.R.J.v. and Lieshout, H.v. (2007). Offshore windpark egmond aan zee - performance of scour protection and edge scour development, In: *Proceedings of the European Offshore Wind Conference 2007 (EOW 2007), Berlin, Germany*, pp 10.

Rance, P. and Warren, N. (1969). The threshold of movement of coarse material in oscillatory flow, In: *Coastal Engineering 1968*, 487–491.

Riezebos, H., Raaijmakers, T., Tönnies-Lohmann, A., Waßmuth, S. and Van Steijn, P. (2016). Scour protection design in highly morphodynamic environments, In: *Proceedings of the 8th International Conference on Scour and Erosion (ICSE-8)*.

Roulund, A., Sutherland, J., Todd, D. and Sterner, J. (2016). Parametric equations for shields parameter and wave orbital velocity in combined current and irregular waves.

Sarmiento, J., Guanche, R., Iturrioz, A., Ojanguren, T., Ávila, A. and Yanes, C. (2021). Experimental evaluation of dynamic rock scour protection in morphodynamic environments for offshore wind jackets. *Energies*, **14**(12), 3379.

Schendel, A., Goseberg, N. and Schlurmann, T. (2014). Experimental study on the performance of coarse grain materials as scour protection, In: *Proceedings of the Coastal Engineering Conference (2014)*, Reston: American Society of Civil Engineers (ASCE).

Schendel, A., Hildebrandt, A., Goseberg, N. and Schlurmann, T. (2018). Processes and evolution of scour around a monopile induced by tidal currents. *Coastal Engineering*, **139**, 65–84.

Schendel, A. and Schlurmann, T. (2019). Subsidence of granular scour protection around a pile exposed to currents, In: *Coastal Structures 2019*, 608–619, Bundesanstalt für Wasserbau.

Schendel, A., Welzel, M., Schlurmann, T. and Hsu, T.W. (2020). Scour around a monopile induced by directionally spread irregular waves in combination with oblique currents. *Coastal Engineering*, **161**, 103751.

Silva-Muñoz, N. and Broekema, Y. (2025). A multi-scale approach for scour time development at monopiles due to currents. *Ocean Engineering*, **322**, 120504.

Soulsby, R.L. and Whitehouse, R.J. (1997). Threshold of sediment motion in coastal environments, In: *Pacific Coasts and Ports' 97: Proceedings of the 13th Australasian Coastal and Ocean Engineering Conference and the 6th Australasian Port and Harbour Conference; Volume 1*, 145–150, Centre for Advanced Engineering, University of Canterbury Christchurch, NZ.

Sumer, B. and Fredsøe, J. (2001*a*). Wave scour around a large vertical circular cylinder. *Journal of Waterway, Port, Coastal and Ocean Engineering*, **127**(3), 125–134. ISSN 0733950x, 19435460. DOI:10.1061/(ASCE)0733-950X(2001)127:3(125).

Sumer, B.M., Christiansen, N. and Fredsøe, J. (1997). The horseshoe vortex and vortex shedding around a vertical wall-mounted cylinder exposed to waves. *Journal of Fluid Mechanics*, **332**, 41–70. ISSN 00221120, 14697645.

Sumer, B.M., Cokgor, S. and Fredsøe, J. (2001). Suction removal of sediment from between armor blocks. *Journal of Hydraulic Engineering*, **127**(4), 293–306. ISSN 07339429, 19437900. DOI:10.1061/(ASCE)0733-9429(2001)127:4(293).

Sumer, B.M. and Fredsøe, J. (2001*b*). Scour around pile in combined waves and current. *Journal of Hydraulic Engineering*, **127**(5), 403–411. ISSN 07339429, 19437900. DOI:10.1061/(ASCE)0733-9429(2001)127:5(403).

Sumer, B.M. and Fredsøe, J. (2002). *The mechanics of scour in the marine environment*, World Scientific, advanced series on ocean engineering : 17.

Sumer, B.M., Fredsøe, J. and Christiansen, N. (1992). Scour around vertical pile in waves. *Journal of waterway, port, coastal, and ocean engineering*, **118**(1), 15–31.

Sumer, B.M., Petersen, T.U., Locatelli, L., Fredsøe, J., Musumeci, R.E. and Foti, E. (2013). Backfilling of a scour hole around a pile in waves and current. *Journal of Waterway, Port, Coastal, and Ocean Engineering*, **139**(1), 9–23.

Umeda, S. (2011). Scour regime and scour depth around a pile in waves. *Journal of Coastal Research*, 845–849.

Umeda, S. (2013). Scour process around monopiles during various phases of sea storms. *Journal of Coastal Research*, (65), 1599–1604.

van Steijn, P.W., Wu, M. and Broekema, Y. (2023). Towards a better understanding of loose rock scour protection stability around monopile foundations, In: *11th International Conference on Scour and Erosion*, International Society for Soil Mechanics and Geotechnical Engineering.

Vithana, H.P.V. (2013). *The effect of stone protrusion on the incipient motion of rock armour under the action of regular waves*, Ph.D. thesis, UCL (University College London).

Whitehouse, R., Brown, A., Audenaert, S., Bolle, A., de Schoesitter, P., Haerens, P., Baelus, L., Troch, P., Das Neves, L., Ferradosa, T. et al. (2014). Optimising scour protection stability at offshore foundations, In: *Proceedings of the 7nd International Conference on Scour and Erosion (ICSE-7)*, 593–600.

Whitehouse, R.J., Harris, J.M., Sutherland, J. and Rees, J. (2011). The nature of scour development and scour protection at offshore windfarm foundations. *Marine Pollution Bulletin*, **62**(1), 73–88. ISSN 0025326x, 18793363. DOI:10.1016/j.marpolbul.2010.09.007.

Willis, D. (1978). Sediment load under waves and currents, In: *Coastal Engineering 1978*, 1626–1637.

Wu, M., De Vos, L., Arboleda Chavez, C.E., Stratigaki, V., Fazeres-Ferradosa, T., Rosa-Santos, P., Taveira-Pinto, F. and Troch, P. (2020). Large scale experimental study of the scour protection damage around a monopile foundation under combined wave and current conditions. *Journal of Marine Science and Engineering*, **8**(6), 417.

Yao, W., An, H., Draper, S., Cheng, L. and Harris, J.M. (2018). Experimental investigation of local scour around submerged piles in steady current. *Coastal Engineering*, **142**, 27–41.

Appendix

A Calculating u_m in irregular waves

In this article the oscillatory flow induced by irregular waves is, unless noted otherwise, defined as:

$$u_m = \sqrt{2}\sigma_u \tag{25}$$

where

$$\sigma_u^2 = \int_0^\infty S_u(f)df \tag{26}$$

where S_u is the power spectrum of the velocity calculated using linear wave theory:

$$S_u = \left(\frac{\omega \cosh(k(z+h))}{\sinh(kh)}\right)^2 S_f \tag{27}$$

where S_f is the power spectrum of the surface elevation, in the present case a standard JONSWAP spectrum is applied, $\omega = 2\pi f$ is the angular wave frequency, h is the water depth outside the scour protection, z is measured from the initial top of the scour protection, and k is the wave number defined as:

$$\omega^2 = gk\tanh(kh) \tag{28}$$

where g is the acceleration due to gravity.

B Calculating bed shear stress in combined waves and current

The maximum bed shear stresses for combined waves and current, τ_{max}, are calculated using the method proposed by Roulund et al. (2016). The method is outlined in the following:

$$\tau_{max} = \tau_m + \tau_w \tag{29}$$

where τ_w is the bed shear stress due to waves and τ_m is defined as:

$$\tau_m = \tau_c \left(1 + 1.2 \left(\frac{\tau_w}{\tau_c + \tau_w} \right)^{3.2} \right) \tag{30}$$

where $\tau_c = \rho_w U_f^2$ and ρ_w is the density of the water and U_f is the current induced friction velocity:

$$U_f = \frac{V}{6.0 + 2.5 \ln(h/k_s)} \tag{31}$$

where h is the water depth (see Fig. 1) and $k_s = 2.5 D_{50}$ where D_{50} is the median rock size.

The wave induced bed shear stress, τ_w is calculated as:

$$\tau_w = 0.5 \rho_w f_w u_m^2 \tag{32}$$

where u_m is the amplitude of the wave induced velocity as defined in App. A. The velocity shall be calculated for the water depth at the surround seabed, h in Fig. 1 while $z = -(h - t_{sp})$, again, see Fig. 1.

The wave friction factor, f_w, is calculated as:

$$f_w = \begin{cases} 0.32 \left(\frac{A}{k_s} \right)^{-0.8} & \text{for } 0.2 < \left(\frac{A}{k_s} \right) < 2.92 \\ 0.237 \left(\frac{A}{k_s} \right)^{-0.52} & \text{for } 2.92 \leq \left(\frac{A}{k_s} \right) < 727 \\ 0.04 \left(\frac{A}{k_s} \right)^{-0.25} & \text{for } \left(\frac{A}{k_s} \right) \geq 727 \end{cases} \tag{33}$$

where A is the amplitude of the wave motion:

$$A = \frac{u_m T_p}{2\pi} \tag{34}$$

C Procedure for calculating equilibrium deformation and time scale

The procedure for calculating the equilibrium deformation and the time scale is outlined in this appendix. As shown in Sec. 4.3.1 it is important to apply the same procedure for the calculations to ensure the correct input for the empirical formulae to provide as accurate as possible results. When calculating the relative equilibrium deformation and the time scale using the methods proposed in this article, the following procedure shall be applied:

1. Determine the depth average current velocity, V (it shall be averaged over the depth, h, as defined in Fig. 1. It is assumed that the boundary layer is fully developed over the entire depth.
2. Calculate the wave induced velocity, u_m, as outlined in App. A. The velocity shall be calculated for the water depth at the surround seabed, h in Fig. 1 while $z = -(h - t_{sp})$, again, see Fig. 1.
3. Determine the maximum bed shear stress, τ_{max}, as defined in App. B where $k_s = 2.5 D_{50}$ and D_{50} is the median rock size of the scour protection.
4. Calculate the Shields number: $\theta = \tau_{max}/(\rho_w g(s-1) D_{50})$ where ρ_w is the density of the water, g is the acceleration due to gravity, and s is the specific density of the rock.
5. Calculate the wave-current ratio: $u_{cw} = V/(V + u_m)$.
6. Calculate the relative equilibrium deformation, S/D_p using Eq. 7.
7. Calculated the dimensionless time scale, T^*, using Eq. 15 with parameters as defined in Eq. 16 as well as $\Psi_c = 0.02$, $b_1 = 0.36$, and $b_2 = 5$
8. Calculate the time scale using Eq. 10